Energetics and intramolecular dynamics of the isolated ultracold tetracene molecule in its first excited singlet state

A. Amirav, U. Even, and Joshua Jortner

Department of Chemistry, Tel-Aviv University, Tel Aviv, Israel
(Received 30 September 1980; accepted 9 December 1980)

In this paper we report the results of an experimental study of the energetics and intramolecular dynamics of the first electronically excited S_1 singlet state of tetracene ($C_{18}H_{12}$) seeded in supersonic expansions of rare gases. Internal cooling of tetracene in supersonic expansions of Ar down to rotational temperatures $T_R \sim 5$–7 K and vibrational temperatures $T_V < 50$ K can be accomplished at moderately low stagnation pressures $p = 100$–200 Torr of Ar, Kr, and Xe when expanded through a $D = 150\,\mu$ nozzle. We have interrogated the fluorescence action spectra, the energy-resolved fluorescence, and the time-resolved fluorescence of the ultracold, isolated, bare, large molecule for excess vibrational energies $E_V = 0$–4000 cm^{-1} above the electronic origin of the S_1 state. The electronic origin of the $S_0(^1A_{1g}) \rightarrow S_1(^1B_{2u})$ transition located at 22 360 cm^{-1} exhibits a partially resolved B-type rotational structure, which concurs with the short axis polarization of this transition. We were able to identify nine totally symmetric a_{1g} fundamentals and three vibronically induced b_{3g} fundamentals in the vibrational structure of S_1 in the energy range $E_V = 0$–1600 cm^{-1}. The vibrational structures of the S_1 state and of the S_0 state in the isolated molecule are in good agreement with the mixed crystal data, indicating small medium effects on the low-energy vibrational level structure. Information on the shift and distortion of the potential surface of the S_1 state relative to S_0 was inferred from frequency changes and from Franck–Condon vibrational overlap factors. We have investigated two classes of nonreactive dynamic processes in the S_1 manifold, involving intrastate anharmonic mixing (IAM) and interstate electronic relaxation (ER). IAM was explored by the observation of the onset for spectral congestion in the absorption spectrum which marks the onset of the vibrational quasicontinuum, as well as by the observation of band splitting in the energy-resolved emission spectra which marks the onset of IAM. The threshold for IAM in the S_1 state of tetracene is exhibited at $E_V \simeq 1000$ cm^{-1} below the onset of the vibrational quasicontinuum, which occurs at $E_V \simeq 1600$–1800 cm^{-1}. These observations provide a firm basis for the identification of three energy regions for IAM in the S_1 manifold of this large molecule, i.e., the sparse level structure ($E_V = 0$–1000 cm^{-1}), the intermediate level structure ($E_V = 1000$–1600 cm^{-1}), and the statistical limit ($E_V > 1800$ cm^{-1}). Information concerning ER in the S_1 manifold was obtained from the experimental decay lifetimes τ of photoselected states at excess vibrational energies $E_V = 0$–4000 cm^{-1}. Excitations in the sparse vibrational level structure in the range $E_V = 0$–1200 cm^{-1} results in a retardation of the ER rate relative to its value for the electronic origin; this blocking of the ER rate for low E_V is attributed to $S_1 \rightarrow T_1$ intersystem crossing, which is characterized by a low electronic energy gap. Excitation in the vibrational quasicontinuum results in the τ values which are practically independent of E_V with $\tau = 4.5 \pm 0.5$ nsec in the range $E_V = 2000$–4000 cm^{-1}. This observation cannot be reconciled with the notion of effective energy redistribution among all vibrational modes and is tentatively attributed to the effects of selective intrastate anharmonic mixing which involves a subset of the vibrational states.

I. INTRODUCTION

High-resolution electronic spectra of large molecules in the low-pressure gas phase are usually diffuse.[1] The spectral diffuseness may be due to homogeneous broadening originating from intramolecular nonradiative relaxation processes, e.g., electronic relaxation or predissociation.[1–5] Alternatively, spectral diffuseness may be due to a large number of rotational–vibrational transitions. Thermal populations of rotational and vibrational levels of the ground electronic state, together with angular momentum selection rules for rotational excitation and in conjunction with the propensity rule $\Delta v = 0$ for the excitation of each of the nonsymmetric vibrational modes, result in appreciable thermal inhomogeneous broadening (TIB) effects. These TIB effects obscure most of the vibrational structure in electronically excited states of large molecules studied in the gas phase. To overcome these effects of TIB on the absorption spectra, it was customary to conduct spectroscopic studies on guest molecules in low-temperature mixed crystals[6] and in Shpolskii matrices.[7] The identification of the zero-phonon lines of the guest molecule contributed substantially to the elucidation of excited-state energetics. However, the spectroscopic and the dynamic information emerging from such studies is inherently complicated because of four reasons: (a) site splitting due to different trapping sites,[8,9] (b) inhomogeneous broadening originating from statistical distribution within each trapping site,[8,9] (c) lattice multiphonon side bands,[10] and (d) medium-induced vibrational relaxation of vibrationally excited molecular states.[8,9] The last point brings up a basic difficulty in probing intramolecular dynamics of large molecules when embedded in a dense medium. During the last decade there has been considerable experimental and theoretical efforts aimed towards the understanding of nonreactive relaxation phenomena, i.e., interstate electronic relaxation and intrastate vibrational energy redistribution in electronically and vibrationally excited states of large molecules.[2–5,11–18] Pertinent information concerning these phenomena stems from the interrogation of time-resolved or energy-resolved decay of well-defined photoselected molecular states of "isolated" collision-free large molecules. The "isolated" molecule limit can be accomplished in some carefully designed bulb experiments[2,15,18] and in thermal molecular beams.[19,20] However, photoselective excita-

 0021-9606/81/203770-24$01.00

tion of a well-defined initial state of a large molecule cannot be accomplished in such bulb or beam experiments conducted at room temperature, as the molecule carries its memory of thermal population of the ground state to the electronically excited state. The severe effects of TIB obscure the dynamic as well as the energetic information pertaining to electronically excited states of isolated large molecules. A powerful way to overcome TIB effects rests on the use of isentropic supersonic expansions advanced by Kantrowitz and Grey 30 years ago.[21] The spectroscopic implications of supersonic expansions were recognized by Huber and Douglas,[22] who proposed that supersonic-free expansion of a polyatomic gas can lead to appreciable rotational and vibrational cooling, thus resulting in a considerable simplification of the notorious absorption spectra of some triatomic molecules, such as NO_2. These pioneering studies of absorption spectroscopy in supersonic expansions conducted in 1963–1965 demonstrated the rotational cooling of NO and NO_2. The merger between laser technology and supersonic beams led to remarkable progress in spectroscopy. This technique was advanced by Sinha, Schultz, and Zare for the study of alkali dimers[23] and by Smalley *et al.* for the investigation of NO_2.[24,25] The use of supersonic-free expansions of seeded molecular beams results in ultracold, "isolated," large molecules, whose excited-state energetics and dynamics can be explored experimentally.[26–42] In this paper, we report the results of our experimental study of the energetics and intramolecular dynamics of the first electronically excited singlet state S_1 of the tetracene ($C_{18}H_{12}$) molecule seeded in supersonic molecular beams of rare gases. A preliminary report of some of these results was presented already,[29,39] while in the present paper a full account of the energetic and dynamic information is unveiled. The technique used by us[38] rests on expanding the large and heavy molecule in heavy rare-gas diluents, e.g., Ar and Kr through nozzles of diameters $D = 100–200\ \mu$. Efficient cooling of the internal degrees of freedom of the heavy molecule in the supersonic expansion of heavy diluents down to rotational temperatures of $T_R \sim 5–7$ K and to vibrational temperature of $T_V < 50$ K can be accomplished at moderate values ($p = 150–250$ Torr) of the stagnation pressure of the heavy rare gas. Excited-state energetics in the S_1 state was interrogated by monitoring the energy-resolved fluorescence action spectra, and additional energetic data were obtained from energy-resolved fluorescence spectroscopy. This energetic information provides input data, which are essential for the elucidation of excited-state intramolecular dynamics. We are interested in two general classes of nonreactive relaxation phenomena in bound electronically and vibrationally excited states of large molecules,[2–5,11–18] i.e., interstate electronic relaxation (ER) and intrastate vibrational energy redistribution (IVR). Direct spectroscopic information on IVR, i.e., anharmonic mixing within the S_1 manifold of tetracene, was obtained from the fluorescence action spectrum, as well as from studies of the energy-resolved fluorescence. The present study provides an unambiguous identification of the threshold for intrastate anharmonic coupling, as well as the observation of the onset of the vibrational quasicontinuum in the S_1 state of this large molecule. This information is pertinent for the understanding of the broad class of phenomena pertaining to IVR that are of central importance in the areas of unimolecular reactions[43] and high-order multiphoton excitation.[44,45] While the features of IVR are not yet fully elucidated, the problems of interstate coupling and ER in isolated molecules were extensively explored.[2–5,11–18] The present work provides new information on ER of photoselectively excited vibrational states in the S_1 manifold of the tetracene molecule. The time-resolved decay lifetimes of well-defined photoselected vibrational states within the S_1 manifold of this large molecule drastically differ in respect to their absolute values, as well as in their dependence of the excess vibrational energy, from the lifetimes obtained in low-pressure bulb experiments at elevated temperatures. From the experimental point of view, our data demonstrate the nature of the novel information on ER of isolated large molecules which cannot be obtained under conventional circumstances. From the point of view of general methodology, our experimental lifetime data indicate that the details of the current theories of optical selection in ER require some gross modifications. The results of the present study demonstrate that the increase of spectral resolution in seeded supersonic beams by three orders of magnitude over that accomplished in bulb experiments and in thermal effusive beams provides a powerful method for genuine photoselective excitation of well-defined vibrationally and electronically excited states of large isolated molecules and for the interrogation of the dynamic consequences of such photoselective excitation, a goal which could not be accomplished previously under conventional circumstances.

II. EXPERIMENTAL PROCEDURES

A schematic presentation of the apparatus for laser spectroscopy of large and heavy molecules in seeded supersonic beams is presented in Fig. 1. We shall now proceed to describe in some detail the components of our system.

A. Pumping

Our supersonic beam apparatus uses a pumping system constituting a 6-in. diffusion pump (Varian VHS 6), backed by a rotatory pump (Alcatel) with a pumping speed of 500 $\ell\ \text{min}^{-1}$. This pumping system was utilized for supersonic-free expansions of seeded Ar, Kr, and Xe through 150 μ and 200 μ nozzles at stagnation pressures of $p = 50–1000$ Torr. Spectroscopic and lifetime studies were usually conducted at $p = 200$ Torr of Ar. For some high-flow experiments,[38] where He was expanded at $p = 7600$ Torr through a 150 μ nozzle, only the Alcatel rotatory pump was employed.

B. Nozzles

The supersonic nozzles were of two types: (a) A 160-μ nozzle was mechanically drilled and chemically etched in a 100-μ thick Tantalum disk. (b) A ceramic 200-μ nozzle was built from machinable ceramic in order to eliminate the possibility of thermal decomposition of the

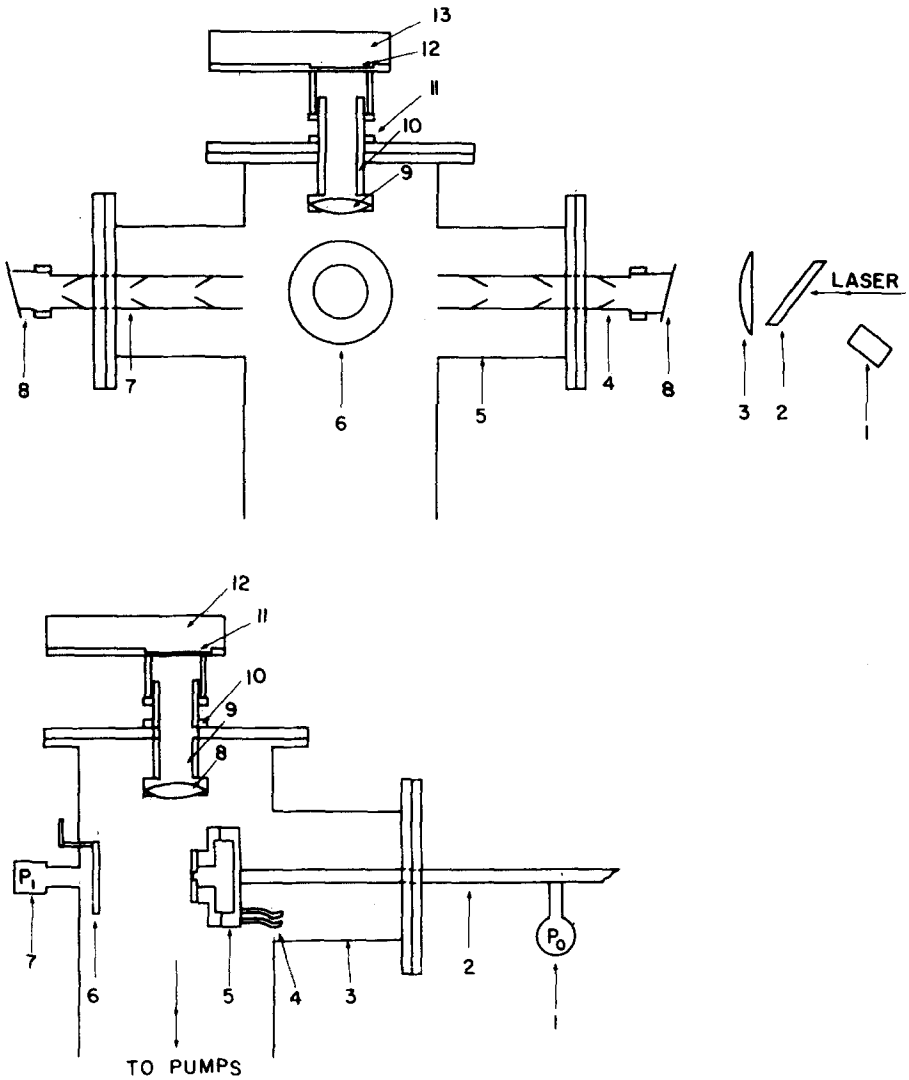

FIG. 1. The basic experimental arrangement for laser spectroscopy in seeded supersonic expansions. The upper part describes the setup for laser excitation and interrogation. The components of the system are 1. energy meter, 2. beam splitter, 3. focusing lens, 4. light baffles, 5. vacuum envelope, 6. oven and nozzle, 7. light baffles, 8. vacuum window, 9. light collection lens, 10. lens holder, 11. vacuum seal, 12. filter holder, 13. photomultiplier. The lower part describes schematically the gas feeding system. The components are 1. pressure gauge, 2. gas supply tube, 3. vacuum chamber, 4. thermocoax and thermocouple, 5. oven and nozzle, 6. beam flag, 7. ionization gauge, 8. collection lens, 9. lens holder, 10. vacuum seal, 11. filter holder, 12. photomultiplier.

tetracene molecule on the metal surface. The nozzle hole was backed by a piece of sinterglass to prevent clogging of the nozzle.

The nozzle oven was constructed out of two standard ultrahigh vacuum 3-in. flanges. These flanges were heated by a thermocoax. The temperature was controlled by a Eurotherm controller. The oven was radiation shielded to decrease the effects of black-body radiation on the photomultiplier.

C. Beam production

A gaseous mixture of the diluent gas and the tetracene molecule was expanded through the nozzle. The diluent gas consisted of Ar or Kr at $p = 20-500$ Torr. The tetracene sample (purchased from Aldrich and used without further purification) was mass analyzed for purity. The tetracene powder was heated to 220 °C, where the vapor pressure is about 0.1 Torr. The diluent gas was sent through the heated nozzle chamber containing the solid sample of tetracene.

D. Diluent gas

We have found that the mass of the diluent rare gas exhibits a marked effect on the degree of rotational–vibrational cooling of the large molecule.[38] Efficient rotational–vibrational cooling was accomplished with Ar and Kr at moderate values of $pD = 2-3$ Torr cm, where D is the nozzle diameter. This effective internal cooling at moderate values of pD in heavy diluents cannot be accomplished in a light diluentlike He under the same conditions because of the velocity slip effect.[38,46-48] The customary use of He as a diluent requires a large throughput pumping apparatus[24-27] or a pulsed nozzle source. Our technique, based on the use of the heavy diluents, makes it possible to use a "poor man's" medium-sized pumping throughput setup (see Sec. II A) in the construction of the supersonic beam apparatus. By an optimal choice of the stagnation pressure of Ar and Kr in the range $p = 100-300$ Torr, internal cooling was accomplished, and the spectrum was not obscured by the formation of van der Waals complexes between the aromatic molecule and the rare-gas atoms.[38]

E. Collision-free conditions

The dynamic studies interrogating excited-state lifetimes and energy-resolved fluorescence were conducted in seeded supersonic expansions of Ar at the stagnation pressure of $p \simeq 200$ Torr. Under these conditions the

pressure on the vacuum chamber is $p_1 \simeq 10^{-3}$ Torr. The Mach disk[49] appearing at the distance $X_M = 0.67\, D(p/p_1)^{1/2}$ from the nozzle will be exhibited at $X_M = 50$ mm, establishing the boundary of the "zone of silence."[49] The interrogation of excited-state dynamics by laser spectroscopy was conducted at a distance $X = 5-7$ mm from the nozzle, i.e., $X/D = 30-40$. The density, ρ, in the interrogation range is[49] $\rho = 0.16\, \rho_0 (X/D)^{-2}$, where ρ_0 is the stagnation density. The time, τ_c, between collisions is $\tau_c = \lambda/\Delta v$, where λ is the mean free path and $\Delta v = (v/M)$, being the spread of the velocity around the mean value $v = (5kT_0/\mu)^{1/2}$, M is the Mach number, T_0 is the nozzle temperature, and μ represents the mass of the diluent, Taking $\lambda = 1/\sigma\rho$, where σ is a typical collisional cross section, we get $\tau_c = M/V\sigma\rho$, and utilizing the relations[26] $M = 133\ (PD)^{0.4}$ for Ar and the density relation, we finally get

$$\tau_c = \frac{133(PD)^{0.4}(X/D)^2}{[(5kT_0/\mu)^{1/2}]\,\sigma 0.16\,\rho_0}\ .$$

Typical values are $T_0 = 500$ K, $\rho_0 = 5\times 10^{18}$ cm^{-3}, $pD = 4 \times 10^{-3}$ atm cm, $M = 14.5$, and $X/D = 33$. Taking a large collisional cross section of $\sigma = 250$ Å^2, we finally obtain $\tau_c = 10^{-5}$ sec. As the experimental lifetimes are $\tau \leq 30$ nsec, which are considerably shorter than τ_c, the tetracene molecule can be considered to be "isolated" on the relevant time scale.

F. Dye laser

We have used a pulsed nitrogen pumped dye laser (Molectron DL2) with a spectral bandwidth of 0.3 cm^{-1} (as specified by the manufacturer). The temporal laser pulse width (FWHM) measured by a fast photodiode and a sampling scope was 4.0 ± 0.5 nsec. The temporal response of the entire measuring system to be described in Sec. II H was somewhat longer. The laser was passed through a polarizer to reduce the effects of the laser superradiance. A small portion of the laser beam was split and directed onto a detector for continuous monitoring of the intensity. The signal of the detector was used for the on-line normalization of the fluorescence action spectra to the laser intensity. The laser beam was focused into the vacuum chamber. In order to eliminate spurious effects of laser stray light, the laser beam was baffled at the entrance and at the exit tubes, which are connected to the vacuum system. The laser crossed the seeded supersonic beam at the distance $X = 5-7$ mm from the nozzle; this distance could be controlled by moving the nozzle. The absolute laser wavelength was calibrated utilizing the photogalvanic effect, as well as by a conventional technique using a monochromator (1/4 m McPherson). The accuracy of the absolute wavelength scale is ± 3 Å, the absolute accuracy of the frequency scale being ± 15 cm^{-1}. A schematic outline of the setup for spectroscopic measurements and for the interrogation of energy-resolved and time-resolved fluorescence following laser excitation of the seeded supersonic beam is outlined in Fig. 2.

G. Fluorescence action spectra

These correspond to the intensity of the total fluorescence versus the laser wavelength, which was continuously scanned. The total fluorescence was collected through a light pipe (diameter 6.3 mm) or by a $f = 1$ lens (focal length 35 mm). In earlier experiments we used the light pipe which was placed approximately 8 mm above the nozzle and which was heated to prevent condensation of the tetracene. In subsequent experiments the light collecting lens was preferred. The collected fluorescence was passed through glass filters to eliminate stray light and detected by a fast photomultiplier (Hammamatsu R-936 or Phillips XP 1021). The photomultiplier output was recorded by a boxcar integrator after normalization to the laser intensity. The spectra were recorded by an x-y recorder. The x axis, corresponding to the laser wavelength, was controlled by the computer (HP model 9825 A), which also controlled the laser scan. The y axis corresponds to the fluorescence intensity divided by the laser intensity. The spectra presented in the present work provide a faithful reproduction of the scans of the x-y recorder.

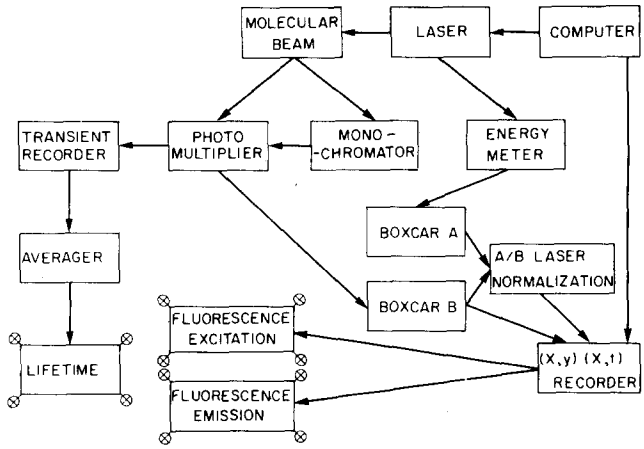

FIG. 2. A schematic block diagram of the setup for the interrogation of fluorescence action spectra, energy-resolved emission, and time-resolved emission in seeded supersonic expansions.

H. Energy-resolved fluorescence spectra

These correspond to the energy-resolved fluorescence resulting from excitation at a fixed laser wavelength. The energy-resolved laser-excited fluorescence from the seeded jet was collected and imaged by a lens onto the entrance slit of a monochromator (Jarrel-Ash 1/4 m) and detected by a Hammamatsu photomultiplier, the resulting spectra resolution being 7 Å (30 cm^{-1}). The spectra were recorded by the x-y recorder. Effort was devoted to the characterization of the emission signal at the laser wavelength, which can originate from three sources: (a) resonance fluorescence, (b) near-resonant Rayleigh (elastic Raman) scattering, and (c) spurious laser stray light. We did not find evidence for the contribution from source (b). Two techniques were applied to distinguish between genuine resonance fluorescence and the laser stray light: (i) We have measured the energy-resolved lifetimes for emission by the techniques to be described in Sec. III. Emission of type (c) follows the temporal decay of the laser pulse, Eq. (II.1), while the temporal duration of the resonance fluorescence and type (a) is characterized by longer exponential fluores-

cence decay times with $\tau \geq 4$ nsec. (ii) When the energy-resolved emission was broad, we were able to determine the nature of the resonant emission signal from the measurement of its energetic width by reducing the slit width of the monochromator. Observation of a resonant signal, whose energetic width is not broadened being equal to the spectral resolution, is assigned to spurious emission of type (c).

I. Lifetime measurements

The time-resolved emission, resulting from excitation at a fixed laser wavelength, was measured by a Biomation (Model 8100) transient recorder and was averaged by a home-built signal averager. The spacing between consecutive channels of the transient recorder was 10 nsec. The temporal response function $F(t)$ of the measuring system (laser width, laser jitter, photomultiplier rise and fall time, and Biomation) could adequately be represented by a Gaussian function

$$F(t)\exp[-\alpha^2(t-t_0^2)]\,, \tag{II.1}$$

with $\alpha = 0.10$ nsec^{-1} and the pulse width (FWHM) being $(\ln 2)^{1/2}\alpha^{-1} = 8$ nsec. t_0 marks the time (on a relative scale) corresponding to the maximum of the pulse. The decay of the fluorescent signal was followed over two to three orders of magnitude. Usually about 3000 fluorescence pulses were averaged for each decay curve. The analysis of the experimental time-resolved decay curves rests on the conventional deconvolution procedure, where the fluorescence signal $I(t)$ at time t is expressed in terms of the convolution of the response of the system to the laser pulse $F(t)$, Eq. (II.1), and the response function $G(t)$ of the system

$$I(t) = \int_0^t dt'\, F(t')\, G(t-t') \tag{II.2}$$

for a single exponential decay $G(t) \propto \exp(-t/\tau)$, being characterized by the lifetime τ. The fluorescence signal (apart from irrelevant numerical constants) is

$$I(t) = \exp[-(t-t_0)/\tau]H(t)\,, \tag{II.3}$$

where

$$H(t) = \tfrac{1}{2}\{\mathrm{erf}[\alpha(t-t_0) - (2\alpha\tau)^{-1}] + \mathrm{erf}[\alpha t_0 + (2\alpha\tau)^{-1}]\}\,. \tag{II.4}$$

The experimental decay curves $I(t)$ can be deconvoluted by calculating the function $I(t) = [H(t)]^{-1}I(t)$ which, according to Eq. (II.3), will directly result in the decay lifetime. Numerical simulations of Eq. (II.3) for the characteristic temporal reciprocal width $\alpha = 0.10$ nsec^{-1} of our laser indicate that in the time domain, where the laser intensity has decayed to values less than 2% of the peak value, i.e., $F(t)/F(t_0) < 0.02$, the correction function is lower than 1.17 for $\tau = 4.0$ nsec and lower than 1.08 for $\tau = 5$ nsec. Thus for $\tau \geq 5.0$ nsec the convolution procedure is not necessary; while for lifetimes in the range $\tau = 4.0$–5.0 nsec direct measurement of τ from the experimental fluorescence decay curves in the time domain where $F(t)/F(t_0) < 0.02$ introduces an upper bound for the systematic error which is 8% for $\tau = 5$ nsec. The experimental lifetime data reported in the present work are believed to be accurate within ± 10% for $\tau \geq 5$ nsec, while for lifetimes in the range $\tau = 4$–5 nsec the accuracy of the lifetime data is ± 15%.

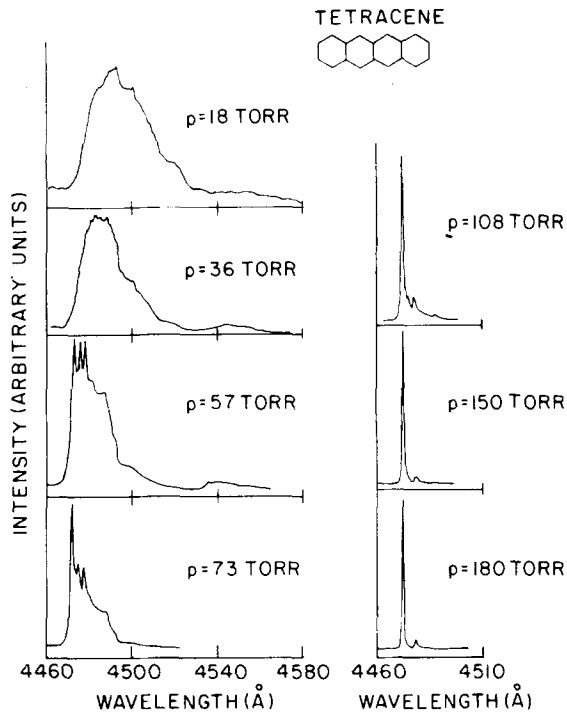

FIG. 3. Fluorescence excitation spectra in the range 4460–4500 Å of tetracene seeded in supersonic expansion of Ar. Tetracene heated in the sample chamber to 220°C (vapor pressure 10^{-1} Torr) was seeded in Ar at backing pressures of 18–180 Torr (indicated on the spectra). The mixture was expanded through a $D = 150$ μ nozzle. The exciting dye laser has a bandwidth of 0.3 cm^{-1} and crossed the supersonic expansion at 5–7 mm down the nozzle. All fluorescence excitation spectra are normalized to the laser intensity. At lower values of $p < 100$ Torr the vibrational sequence congestion and the hot bands are severe; at $p = 180$ Torr the major feature in the spectrum is the 0–0 transition at 4472 Å.

III. COOLING OF TETRACENE IN SUPERSONIC EXPANSIONS

In view of the recent progress in the development of spectroscopic methods in seeded supersonic beams, it is imperative to gain detailed information on the degree of rotational and vibrational cooling of large and heavy molecules in these systems in order to establish the conditions for the reduction of the severe effects of rotational broadening and of vibrational sequence congestion (VSQ). Figures 3 and 4 portray fluorescence excitation spectra of tetracene seeded in Ar at moderate pressures, $p = 18$–200 Torr, and expanded through a $D = 150$ μ nozzle. The excitation spectra of Fig. 3 correspond to the vicinity of the electronic origin of the lowest spin-allowed $^1A_{1g}(v=0) \rightarrow {}^1B_{2u}(v=0)$ electronic transition, which will be discussed in some detail in Sec. IV, as well as to the neighborhood of the first prominent 314 cm^{-1} vibrational excitation of this electronic transition, which appears in Fig. 4. These spectra at low Ar pressures, $p < 100$ Torr, reveal severe effects of rotational broadening and of VSQ. The effects of VSQ (Figs. 3 and 4) are manifested by (i) sequence broadening of ~ 200 cm^{-1} in the vicinity of room temperature and (ii) the intensity of the genuine 0–0 and 0–314 cm^{-1} transitions at high temperature (Fig. 4) is negligibly small, practical-

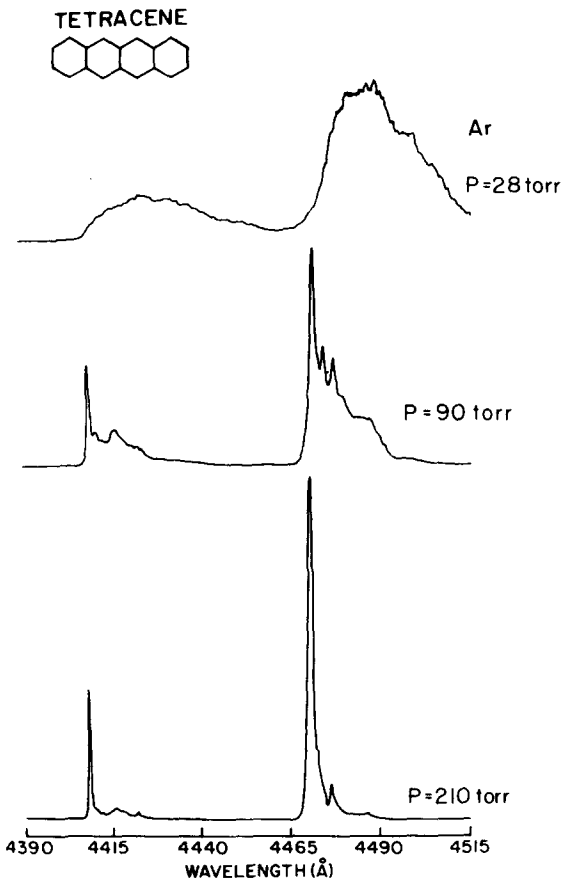

FIG. 4. Fluorescence excitation spectra in the range 4390–4515 Å of tetracene seeded in supersonic expansions of Ar. Argon seeded with 10^{-1} Torr tetracene at three pressures indicated on the spectra was expanded through a $D = 200\ \mu$ ceramic nozzle. These spectra correspond to the electronic origin and to the intense 314 cm^{-1} vibrational excitation of tetracene. Note that the intensity of the 0–0 and of the 0–314 cm^{-1} vibrational features are negligible at a high temperature ($p = 28$ Torr).

ly all the intensity originating from sequence bands. From the results of Figs. 3 and 4, it is apparent that supersonic expansion of tetracene seeded in Ar at the backing pressure of 180 Torr through a $D = 150\ \mu$ nozzle results in an excitation spectrum which is practically free from VSQ. The only alien feature in the excitation spectrum in the vicinity of the 0–0 transition of tetracene in Ar is the peak at 4479 Å (see spectrum at $p = 180$ Torr in Fig. 3), which is due to a van der Waals complex (Sec. IV). The weak satellite bands peaking at 4475, 4488, and 4492 Å (Fig. 4) are intrinsic, being due to sequence bands. We conclude that the use of Ar as a diluent for the large molecule at moderate values of $pD = 2.3$ Torr cm results in efficient internal cooling. On the other hand, the expansion of tetracene in He and Ne under the same pD conditions (Fig. 5) results in a spectrum which is heavily smeared by rotational broadening and by VSQ in the case of He. In the case of Ne rotational cooling appears to be more effective; however, the spectrum is still heavily contaminated by VSQ. Effective internal cooling can be accomplished in the heavy diluents where the mass ratio between the diluent and the molecule is not too low, so that the effects of velocity slip[46–48] are small.

Rough estimates of the internal temperatures of the tetracene molecule in the supersonic expansion of Ar at $p = 180$ Torr can be provided. Regarding the rotational temperature T_R, it is reasonable to assume that in the "heavy" Ar diluent T_R is close to the translational temperature T_t, as is the case for diatomic molecules.[50,38] The terminal translational temperature was evaluated according to

$$T_t = T_0 [1 + \tfrac{1}{2}(\gamma - 1) M^2]^{-1} ,$$

where T_0 is the nozzle temperature, M is the terminal Mach number being given[49] for Ar by $M = 133 (pD)^{0.4}$, and $\gamma = \frac{5}{3}$. For tetracene expanded in Ar at $pD = 2.3$ Torr cm, we calculate $T_t = 7$ K and assert that $T_R \sim 7$ K. As far as the vibrational temperature T_V is concerned, one can utilize the intensity of the sequence bands for an estimate of an upper limit for T_V. The spectrum in Ar at $pD = 2.3$ Torr cm (Fig. 5) reveals a weak sequence band at 4475 Å, separated by 15 cm^{-1} from the origin and characterized by a relative intensity of < 0.01 relative to the 0–0 transition. The lowest ground state vibrational frequency for such an aromatic hydrocarbon is expected to be ~ 200–250 cm^{-1} and, provided that such frequency is responsible for the weak sequence band, we estimate $T_V < 50$ K. This cooling of tetracene in supersonic expansions of Ar down to $T_R \sim 7$ K and $T_V < 50$ K,

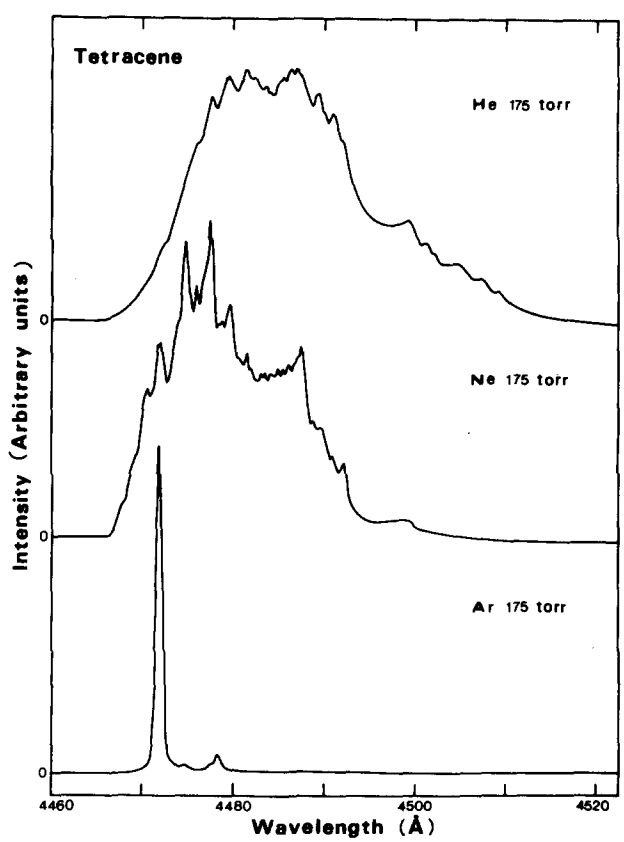

FIG. 5. Fluorescence excitation spectra in the range 4460–4520 Å of tetracene cooled in supersonic expansions of rare gases. Tetracene was seeded into the rare-gas diluent and expanded at a pressure of $p = 175$ Torr through a 150-μ nozzle. The three excitation spectra (from top to bottom) correspond to He, Ne, and Ar, as marked on the figure. The position of the baseline for each excitation spectrum is marked by zero.

accomplished at moderate pressures of heavy diluent, is sufficient to eliminate the effects of VSQ, being adequate for spectroscopic applications and for the study of intramolecular dynamics of photoselected well-defined vibrational states.

IV. SPECTROSCOPY OF THE S_1 STATE OF TETRACENE

A. Spectra of the bare molecule

Figures 6 and 7 show the fluorescence excitation spectra in the range 4500–3800 Å of tetracene seeded in Ar at the stagnation pressure of 180 Torr. We have demonstrated that these spectra originate from the "bare" molecule rather than from van der Waals complexes, which can be formed between tetracene and Ar. The evidence rests on the following observations:

(a) Decreasing the downstream temperature by increasing the Ar pressure in the range 20–180 Torr resulted in rotational–vibrational cooling (discussed in Sec. III); no new intense spectral features were induced by increasing the stagnation pressure. Some weak features, such as band peaking at 4479 Å (Figs. 3–5 and 6) which starts appearing only after vibrational cooling is accomplished, is assigned to the tetracene–Ar complex. However, all the prominent spectral features are due to the bare molecule.

(b) We have conducted a careful comparison between the spectra of tetracene seeded in different diluents, establishing that all the prominent intense features exhibited in the spectra of Figs. 6 and 7 as well as most, but not all, of the weak spectral features are independent of the nature of the carrier gas. The spectral features, which are invariant with respect to the nature of the diluent, originate from the bare molecule. Figure 8 shows a small portion of the spectrum of tetracene in Ar ($p = 180$ Torr), Kr ($p = 135$ Torr), and Xe ($p = 100$ Torr) in the vicinity of the lowest-energy 4472 Å intense

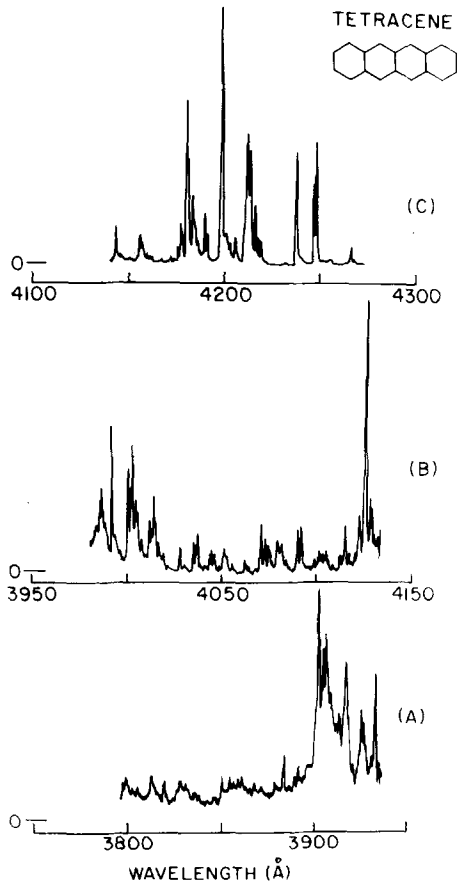

FIG. 7. Fluorescence excitation spectrum in the range 4300–3800 Å of tetracene cooled in a seeded supersonic expansion of Ar at $p = 180$ Torr. The experimental conditions are identical to those of Fig. 3. The fluorescence excitation spectra are normalized to the laser intensity. The relative intensities of two of the spectra relative to the lower spectrum of Fig. 7, which displays the electronic origin, are spectrum (*C*) scaling factor of ($\frac{1}{3}$) and spectrum (*B*) scaling factor of ($\frac{1}{20}$). Spectrum (*A*) is displayed in relative units only. The zero intensity corresponding to the baseline is marked on each of the spectra.

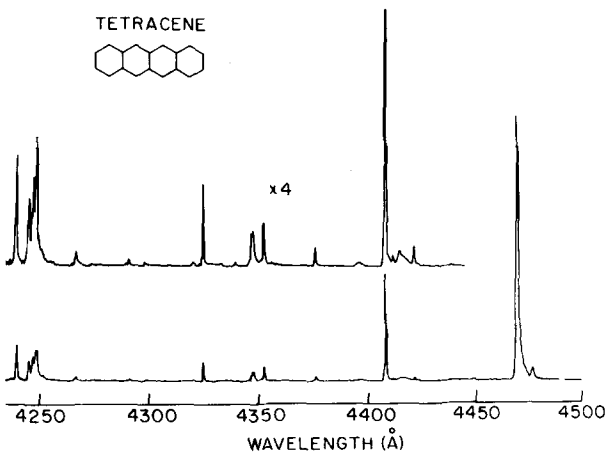

FIG. 6. Fluorescence excitation spectrum in the range 4500–4250 Å of tetracene cooled in a seeded supersonic expansion of Ar at $p = 180$ Torr. The fluorescence excitation spectra are normalized to the laser intensity. The other experimental conditions are identical to those in Fig. 3. The relative intensity (in arbitrary units) at 4500 Å corresponds to the baseline. The relative intensities are marked on the figure.

spectral feature. These spectra clearly demonstrate that the intense 4472 Å feature, which is invariant with respect to the nature of the diluent, originates from the bare molecule. Some very weak bands on the low-energy side depend on the nature of the carrier gas and are due to tetracene-R (R ≡ Ar, Kr, and Xe) van der Waals complexes. A comparison between the spectral features of tetracene expanded in Ar ($p = 175$ Torr) and in He ($p = 7600$ Torr) obtained in the spectral range 4405–4430 Å is displayed in Fig. 9. The prominent spectral feature in this region is the 4410 Å band, which corresponds to the 314 cm^{-1} vibration of tetracene. A careful comparison of the two spectra in Fig. 9 reveals that they are identical, except for the weak band in Ar, which peaks at 4419 Å and which is attributed to the vibrational excitation of the tetracene–Ar complex.

(c) Only at higher stagnation pressures of Ar ($p > 200$ Torr), additional intense new spectral features were exhibited, which are due to tetracene–Ar complexes. The absorption bands attributed to the van der Waals complexes increase fast with increasing pressure. The for-

mation mechanism of these van der Waals complexes involves three-body collisions.[35,38] Accordingly, the intensity of the absorption band due to the tetracene–Ar_n complex is expected to increase with pressure as p^{2n}. This diagnostic criterion[35] is borne out by the new features appearing at $p > 200$ Torr, providing a direct method for distinguishing between the features of the van der Waals complexes and those of the bare molecule.

On the basis of the foregoing arguments we were able to assign all the intense features in the tetracene spectra of Figs. 6 and 7, as originating from the isolated, bare, ultracold molecule. Furthermore, the identification of some weak molecular features, together with studies of energy-resolved fluorescence reported in Sec. IV D, enabled us to identify some weak features in the low-energy range of the spectrum (Fig. 9) as corresponding to vibrational excitation of the bare molecule.

B. The electronic origin

No intrinsic, bare, molecule features were observed at wavelengths below 4475 Å. The lowest-energy spectral feature of the isolated, bare, tetracene molecule in the supersonic beam is located at 4472 Å (22 361 cm^{-1}). The absolute value of the wavelength scale is accurate within ± 3 Å (± 13 cm^{-1}), being determined by the accuracy of the calibration of the laser wavelength. The 4472 Å (22 361 cm^{-1}) spectral feature is attributed to the electronic origin of the lowest spin-allowed and symmetry-allowed $^1S_0(^1A_{1g}) - {}^1S_1(^1B_{2u})$ electronic transition. The

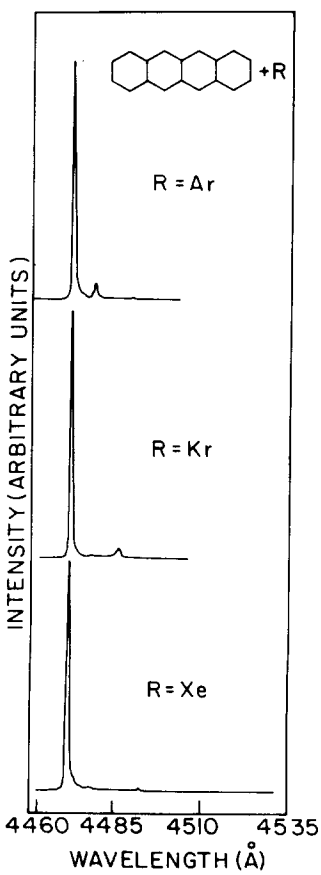

FIG. 8. The fluorescence excitation spectra of tetracene expanded in Ar (p = 180 Torr), Kr (p = 135 Torr) and Xe (p = 100 Torr) in the vicinity of the 0–0 electronic origin of the bare tetracene molecule. Other experimental conditions as in Fig. 3. Note that the intense 4472 Å feature is independent of the nature of the diluent. The weak satellite bands on the low-energy side, which depend on the nature of the diluent, are due to van der Waals complexes.

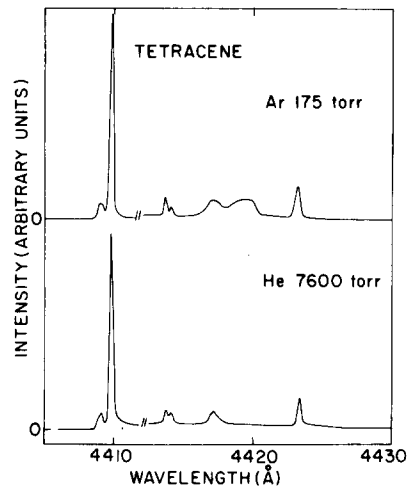

FIG. 9. Fluorescence excitation spectrum of tetracene in the range 4405–4430 Å seeded in a supersonic expansion of He at a backing pressure of p = 10 atm (lower curve) and of Ar at a backing pressure of p = 175 Torr. The nozzle diameter was 150 μ. The high-flow supersonic beam of seeded He (p = 10 atm) was obtained using a mechanical pump with the laser crossing the beam at X = 2.5 mm from the nozzle. The seeded Ar beam at (p = 175 Torr) was crossed by the laser at X = 5 mm from the nozzle. The intensity in the range 4412–4430 Å is scaled up by a numerical factor of 3.0.

B_{2u} symmetry of the electronically excited state[54] in the molecular point symmetry group D_{2h} was unambiguously established on the basis of mixed crystal spectra.[53] The electronic transition moment for this transition is polarized along the short molecular axis. Additional support for this symmetry assignment of the electronic transition originates from the partially resolved rotational structure of the electronic origin. In Fig. 10 we display the fluorescence excitation spectrum of the electronic origin as well as of the 314 cm^{-1} vibration of the tetracene molecule under medium-resolution conditions allowed by the 0.3 cm^{-1} spectral bandwidth of the laser. The individual spectral features in Fig. 10, as well as other spectral features in the low-energy range of the spectrum (Fig. 11), have a width of ~ 3 cm^{-1} because of unresolved rotational structure. An additional cause of broadening of the individual spectral features can be due to the presence of 1.1% of ^{13}C in neutral carbon, so that the percentage of isotope ^{13}C impurities in tetracene is 21%. We were unable to identify any isotopic bands under the highest (0.3 cm^{-1}) spectral resolution employed by us.

A partial resolution of the rotational structure of the electronic origin could be accomplished, as is evident from Fig. 10. The band contour of the electronic origin consists of a double hump devoid of a central peak. The tetracene molecule is an asymmetric top with an asymmetry parameter[1] $\mathcal{K} = -0.97$, thus being close to a prolate symmetric top. If the configurational changes accompanying electronic excitation are small, two types of rotational bands are expected.[55] Type A (parallel) bands, where the transition moment is polarized along the axis of the least moment of inertia, show a strong central Q branch flanked on both sides by weaker P and R branches. Type B (perpendicular) bands have an in-

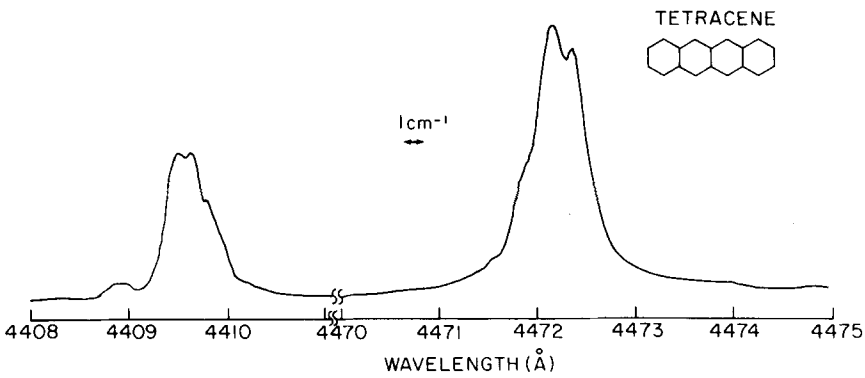

FIG. 10. Medium-resolution fluorescence excitation spectrum (spectral resolution of 0.3 cm^{-1}) of the electronic origin and the 314 cm^{-1} vibration of tetracene cooled in a supersonic expansion of Ar at $p = 180$ Torr. All other experimental conditions as in Fig. 3. Note the B-type rotational structure of the electronic origin.

tensity minimum at the band center flanked by two equidistant intensity maxima. The band contour for the electronic origin of the lowest spin-allowed transition of tetracene conforms to the double-headed perpendicular B band. Accordingly, the double-headed band is short axis polarized. The information stemming from the B-type shape of the rotational contour with regard to the short-axis polarization of the first spin-allowed electronic transition is consistent with the well-established assignment of this electronic excitation to the $^1A_{1g} \rightarrow {}^1B_{2u}$ transition. The largest molecule, whose unresolved rotational structure was reported up to date, is the naphthalene molecule studied by Craig and colleagues.[56] The observation of the rotational structure of the huge tetracene molecule demonstrates again the new possibilities opened up by the advance of the techniques of laser spectroscopy in seeded supersonic beams.

C. Vibrational structure of the S_1 state

The spectrum spanning the range 4500–3850 Å (Figs. 6 and 7) is assigned to the vibrational structure of the lowest spin-allowed $S_0 \rightarrow S_1$ electronic excitation of the tetracene molecule. Tetracene has 15 totally symmetric a_{1g}-type vibrations, all of which are in principle active for the symmetry-allowed $S_0(^1A_{1g}) \rightarrow S_1(^1B_{2u})$ electronic transition. In Table I we present a vibrational analysis of the $S_0 \rightarrow S_1$ electronic transition. In the low-energy range 4500–4410 Å all the bare molecule spectral features were included incorporating both the intense features, i.e., the 4472 Å 0–0 transition and the 4409 Å vibrational excitation at 314 cm^{-1} above the origin, as well as weak spectral features. We have established (see Sec. III) that the very weak features listed in Table I do not originate from van der Waals complexes. However, extreme care must be exerted in the assignment of such weak features to the parent molecule, as they may originate from chemical or isotopic impurities. On the basis of studies of energy-resolved emission, to be reported in Sec. IV D, we were able to attribute the weak features 1a and 2, located at 246 cm^{-1} and at 288 cm^{-1} above the electronic origin, to intrinsic excitation of the tetracene molecule. At higher energies above the 314 cm^{-1} vibration, very weak features were not listed and for the spectral range 4400–3850 Å only the prominent absorption features were incorporated in Table I. The identification of the fundamental vibrations in the S_1 state rests on the following five indicators:

(1) Energetics. In the low-energy range the assignment is quite straightforward.

(2) Relative intensity. In the higher-energy range some of the prominent features are assigned to fundamentals.

(3) Appearance of vibrational progressions and combination bands.

(4) Comparison with the polarized absorption spectrum of tetracene in the mixed crystal.[51–53]

(5) Comparison with the energy-resolved fluorescence spectrum of tetracene in the supersonic expansion (Sec. IV D), which gives information regarding the ground state fundamentals. As the changes in the force constants between the S_0 and the S_1 states are expected to be small, the fundamentals in the ground electronic state and in S_1 are expected to be close in energy.

Twelve fundamental frequencies of the S_1 state were identified. The fundamental frequencies listed in Table II are in good agreement with the S_1 frequencies

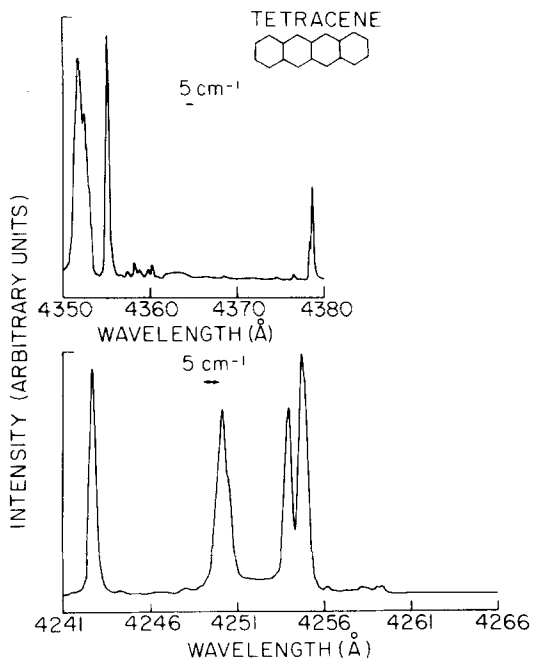

FIG. 11. Some details of the fluorescence excitation spectra of tetracene cooled in Ar at $p = 180$ Torr. All other experimental conditions as in Fig. 3. Note that the four prominent features in the range 4240–4260 Å involve Fermi resonances.

TABLE I. Vibrational assignments and experimental decay lifetimes of the S_1 state of the isolated tetracene molecule.

Number[a] (a)	(Å) λ,[b]	$\Delta\nu = \nu - \nu_{00}$[c] ($cm^{-1}$)	Intensity[d]	Assignment[e,f]	Lifetime[g] (nsec) τ
1	4472.0	0	VS	0–0	20.0
1*a*	4423.3	246	VW		
1*b*	4419.6	265	VW		
2	4415.1	288	VW	288(F)	
3	4410.2	314	S	314(F)	31.8
3*a*	4409.4	317	VW		
4	4378.1	480		480(F)	24.6
5	4355.1	600	S	600(F)	35.7
6	4350.2	626		2×314 – 2	31.0
7	4326.9	750	S	750(F)	34.3
8	4269.7	1060		750 + 314 – 4	21.7
9	4251.7	1159	S	(F) FRS (9–11)	23.8
10	4250.1	1168		FRS (9–11) (?)	28.7
11	4249.2	1173		(F) FRS (9–11)	20.5
12	4239.9	1225	S	1225 (*F*)	20.0
13	4221.6	1323	W	700 + 2×314 + 5	
14	4220.1	1335	W		
15	4218.6	1344		750 + 600 – 6	
16	4215.4	1362	S	1362(F)	23.7
17	4213.5	1372	S	FRS (16–17)	23.4
18	4208.1	1403	W	600 + 480 + 314 + 9	
19	4200.1	1442	S	1442 (F)	21.3
20	4193.0	1488	W	1173 + 314 + 1	
21	4191.0	1499	W	2×750 + 1	
22	4185.7	1529		1529 (F)	
23	4184.0	1539	Sh	1225 + 314	
24	4182.3	1551	S	1551 (F)	14.8
25	4179.5	1565	W		
26	4178.0	1573	W		
27	4158.6	1685		1362 + 314 + 11	12.4
28	4146.0	1758		1442 + 314 + 2	10.6
29	4131.0	1846		1529 + 314 + 3	8.4
30	4128.4	1861	S	1551 + 314 – 4	7.7
31	4118.0	1923			
32	4094.5	2062			
33	4092.5	2074			
34	4073.2	2189		1442 + 750 – 3	6.4
35	4016.6	2536			5.6
36	4005.1	2607			5.1
37	4002.9	2621			5.2
38	3994.4	2673			5.2
39	3988.0	2714		2×1362 – 10	5.0
40	3949.8	2956			
41	3934.4	3056		2×1529 + 2	4.4
42	3927.8	3103		2×1551	4.4
43	3918.7	3158			4.4
44	3907.7	3229			4.2
45	3906.4	3239			
46	3903.8	3245			4.2
47	3885.7	3374			
48	3852.7	3594			4.0
49	3830.7	3744			4.4

[a]The very weak bands 1*b* and 3*a* may be due to impurities. The very weak bands 12 and 2 can safely be assigned to the tetracene molecule on the basis of energy-resolved emission data.
[b]Absolute accuracy of wavelength scale ± 3 Å.
[c]Accuracy of frequencies relative to electronic origin ± 2 cm^{-1}.
[d]Relative intensities are labeled as (VS) = very strong, (S) = strong, (Sh) = shoulder, and (VW) = very weak. The qualitative intensity scale is relative referring separately to each of the four regions in Figs. 6 and 7.
[e]Fundamentals are labeled by (F) and frequencies are expressed in cm^{-1} units.
[f]The occurrence of Fermi resonances is labeled as FRS, where the numbers in parentheses refer to the sequential numbers of those vibrational states which result from the anharmonic mixing. Thus, states 9–11 are mixed and so are states 16 and 17. In these cases, the assignment of fundamental frequencies is somewhat ambiguous.
[g]Accuracy of most lifetimes is ± 10%, and for the short lifetimes in the range 4–5 nsec the accuracy is ± 15%.

TABLE II. A comparison of excited state S_1 fundamentals of the isolated tetracene molecule and of tetracene in mixed crystals.

Symmetry	Isolated molecule (present work)	Host Crystals: p-Terphenyl Ref. (53)	Host Crystals: Naphthalene Ref. (51)	Host Crystals: Dibenzyl Ref. (52)	Host Crystals: Biphenyl Ref. (52)
	314	308	309	314	320
	600	609	619	609	613
	750	746	743	747	747
		755			
		1009			
	1159	1151	1162	1157	1162
a_{1g}	1225	1213	1217	1214	1225
	1362	1361	1358	1365	1376
	1442	1415	1417	1418	1425
	1529	1509	1510	1511	1518
	1551	1549	1563		1562
	288	289			
b_{3g}	480	479		480	
	1173	1166			

from mixed crystal spectra.[51–53] On the basis of the close correspondence between the isolated molecule frequencies and those for the molecule in a mixed crystal spectra can be utilized to distinguish between two types of fundamental frequencies: (i) totally symmetric a_{1g} vibrational frequencies corresponding to the symmetry-allowed $^1A_{1g} \rightarrow {}^1B_{2u}$ electronic transition, and (ii) nontotally symmetric vibrations which derive their intensity via Herzberg–Teller-type vibronic coupling with the higher-energy, strongly allowed $^1B_{1u}$ molecular state. Nine a_{1g} totally symmetric fundamentals were identified at 314 cm^{-1}, 600 cm^{-1}, 750 cm^{-1}, 1159 cm^{-1}, 1225 cm^{-1}, 1362 cm^{-1}, 1442 cm^{-1}, 1529 cm^{-1}, and 1551 cm^{-1}. In addition, three nontotally symmetric fundamental vibrations of 288 cm^{-1}, 480 cm^{-1}, and possibly also 1173 cm^{-1} were observed.

When the excess vibrational energy above the electronic origin increases above 1000 cm^{-1}, interesting complications due to Fermi resonances set in. The three bands (9), (10), and (11) in Table I (see lower part of Fig. 11) are assigned to two fundamentals and a third intense vibrational feature originating from the Fermi resonance, where in this triplet the intensity of a single symmetry-allowed a_{1g} fundamental is shared by all members. Similarly, out of the two strong features (16) and (17) (Table I), one fundamental is effectively coupled to and shares its intensity with its neighbor. The exhibition of these effects of intrastate anharmonic coupling is manifested by three consequences: first, by the modification of the intensity distribution; second, by level shifts; third, by the appearance of new vibrational features. When the excess vibrational energy further increases exceeding approximately 2000 cm^{-1} or so, the effects of intrastate anharmonic coupling result in the appearance of a large number of new vibrational features. This spectral congestion precludes any reasonable vibrational assignment at these higher excess vibrational energies. We shall return in Sec. V to this problem of spectral congestion, which leads to interesting information concerning intrastate vibrational energy scrambling.

D. Energy-resolved emission and vibrational structure of the S_0 state

Figure 12 shows the energy-resolved fluorescence spectrum of the isolated, ultracold, tetracene molecule excited at the electronic origin. This spectrum was obtained under low resolution (30 cm^{-1}), so that the line broadening in the high-energy range of the spectrum is instrumental. The analysis of the vibrational structure of the fluorescence spectrum of Fig. 12 is given in Table III. The intense highest-energy emission band corresponds to the $S_1(v''=0) \rightarrow S_0(v'=0)$ transition, where v'' and v' denote the collection of vibrational quantum numbers in the electronically excited state and in the ground state, respectively. The lower-energy emission bands correspond to the transitions $S_1(0) \rightarrow S_0(v')$, where v' correspond to totally symmetric a_{1g} vibrations for the symmetry-allowed electronic transition, although for Herzberg–Teller induced vibronic components

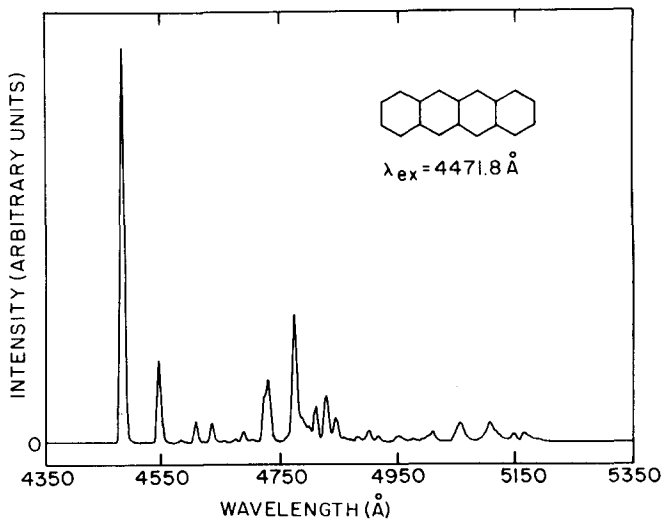

FIG. 12. Energy-resolved fluorescence spectrum of tetracene cooled in a supersonic expansion (180 Torr Ar expanded through a 150-μ nozzle). Photoselective excitation was conducted at the electronic origin (4470 Å). Spectral resolution is 7 Å.

TABLE III. Vibrational analysis of the energy-resolved emission from the electronic origin of S_1 of the isolated tetracene molecule.

λ (Å)[a]	$\Delta\nu = \nu_{00} - \nu$ cm^{-1} [b]	Relative intensity[c]	Assignment
4471.8	0	1.00	0–0
4534.1	307	0.21	F
4571.8	489	0.01	F
4597.7	612	0.01	F and 2×307
4624.3	738	0.05	F
4664.0	922	0.01	612+307 and 3×307
4678.0	986	0.03	F
4944.4	1060	0.01	738+307+15
4714.1	1149	0.12	F
4720.3	1177	0.16	F
4751.0	1314	0.02	
4766.2	1381	0.33	F
4777.6	1431	0.06	F
4789.5	1483	0.04	1177+307
4801.6	1536	0.09	F
4819.9	1615	0.12	F
4836.7	1687	0.06	1381+307
4850.6	1746	0.01	1431+307
4861.7	1793	0.01	1177+612 and 1777+2×307
4874.0	1845	0.02	1536+307
4892.5	1923	0.06	1615+307
4909.3	1993	0.02	1381+612 and 1381+2×307
4943.7	2134	0.02	
4969.1	2238	0.01	
4984.7	2301	0.03	2×1149
5002.3	2372	0.05	2×1177 (?)
5049.5	2558	0.05	
5099.5	2753	0.05	2×1381
5140.9	2911	0.02	
5159.4	2980	0.02	
5181.5	3063	0.01	2×1536
5206.1	3154		

[a]Absolute accuracy of wavelength scale ± 2 Å.
[b]Accuracy ± 10 cm^{-1}.
[c]Relative intensities obtained from the ratio of the amplitudes of the emission peaks in the instrumentally broadened emission spectrum.

v′ will belong to b_{3g} symmetry. As is evident from Table IV, the fundamental vibrations in the S_0 electronic configuration of the isolated, tetracene molecule are very close, within the large experimental uncertainty, to the S_0 frequencies obtained from fluorescence spectroscopy of this molecule in a mixed crystal[51–53] and from Raman spectroscopy of the neat tetracene crystal.[57]

Energy-resolved emission spectroscopy provides a diagnostic tool to determine whether some of the weak low-energy features observed in the fluorescence excitation spectrum (Fig. 9), and which were listed in Table I, originate from the isolated molecule or are due to molecular impurities. Excitation of the tetracene molecule to the $S_1(v_1'')$ electronically and vibrationally excited state is expected to result in an energy-resolved emission spectrum, which is dominated by the transition $S_1(v_i'') \rightarrow S_0(v_i')$, where v_i' is the ground state vibration corresponding to v_i'' in S_1. The prominance of the $\Delta v = 0$ feature, i.e., $S_1(v_i'') \rightarrow S_0(v_i')$ band in the energy-resolved emission spectrum, is characteristic of small configurational changes between the two electronic states of this large molecule. In Fig. 13 we present the energy-resolved fluorescence spectra resulting from photoselective excitation into the very weak feature located at 246 cm^{-1} (band 1b of Table I) and at 288 cm^{-1} (band 2 of Table I), and where we have also displayed for comparison the energy-resolved emission spectra resulting from excitation into the electronic origin and into the 314 cm^{-1} fundamental (band 3 of Table I). The energetic shift $\delta\omega$ between the $\Delta v = 0$ emission and the $S_1(0) \rightarrow S_0(0)$ emission reflects the frequency change $v_i' \omega_i' - v_i'' \omega_i''$ between the frequencies ω_i' and ω_i'' in S_0 and in S_1, respectively. For the $\omega_i'' = 314$ cm^{-1} vibration $\delta\omega \leq 5 \pm 10$ cm^{-1} in accordance with our direct determination (Tables II and IV) that $\omega_i'' = 314 \pm 2$ cm^{-1} and $\omega_i' = 311 \pm 10$ cm^{-1}. For the emission following excitation in the weak 288 cm^{-1} band, we find that $\delta\omega = 10 \pm 10$ cm^{-1}. Two conclusions emerge from this observation. First, we can safely assign the very weak 288 cm^{-1} vibrational feature to an intrinsic fundamental vibration of tetracene. Second, the corresponding ground state vibrational frequency is $\omega_i' = 278 \pm 10^{-1}$. Excitation in the very weak 246 cm^{-1} band results again in an energy-resolved emission spectrum whose general features bear a close resemblance

TABLE IV. Ground state fundamentals of the isolated tetracene molecule and of tetracene in condensed phases (all data in cm^{-1}).

Symmetry	Isolated molecule[a] (present work)	Host crystals: *p*-Terphenyl Ref. (53)	Napthhalene Ref. (51)	Dibenzyl Ref. (52)	Biphenyl Ref. (52)	Neat Ref. (57)
	307	311	321	317	322	317
	612	616	619	618	621	620
	738	758	759	755	759	754
		762				
	986	996	999	998	1003	1000
a_{1g}		1013				
	1149	1154	1162	1162	1166	1165
		1198	1201	1199	1208	1200
	1381	1385	1388	1390	1400	1387
	1431	1446		1448	1455	1451
	1536	1546	1548	1548	1557	1547
	1177	1178				1182
b_{3g}	1615	1615	1621	1622	1629	1621

[a]Accuracy ±10 cm^{-1}.

to that originating from the $S_1(0)$ state, so that it appears that the 246 cm^{-1} vibration is also intrinsic. However, for this excitation $\delta\omega = -50 \pm 10$ cm^{-1}, so that the corresponding ground state frequency is $\omega_i' = 296 \pm 10$ cm^{-1} undergoing a large frequency shift relative to the excited-state frequency. The identification of some very weak features in the energy-resolved spectra, corresponding to the low-frequency molecular vibrations, is of interest for spectroscopic implications, as well as for the elucidation of intramolecular vibrational energy flow in van der Waals complexes between tetracene and rare-gas atoms.[58]

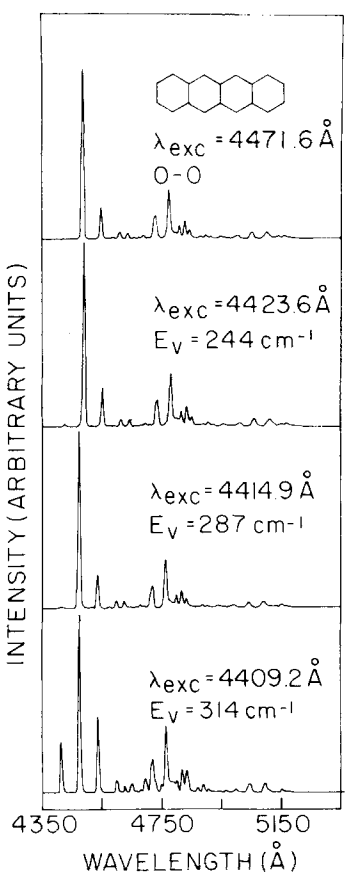

FIG. 13. Energy-resolved fluorescence spectra of tetracene cooled in a supersonic expansion (180 Torr Ar expanded through a 160-μ nozzle). Photoselective excitation was conducted at four excess vibrational energies of (a) $E_V = 0$ (electronic origin (b) $E_V = 246$ cm^{-1}, (c) $E_V = 288$ cm^{-1} and (d) $E_V = 314$ cm^{-1}, which are marked on the spectra.

E. Totally symmetric vibrational fundamentals

From the comparison of the frequencies of the fundamental totally symmetric a_{1g} vibrations in the $S_1(^1B_{2u})$ and in the $S_0(^1A_{1g})$ electronic configurations (Tables III and V) of the isolated tetracene molecule important conclusions emerge concerning intramolecular nuclear motion in the two electronic states. The a_{1g} vibrational frequencies are very close (within 1%) in S_1 and in S_0, clearly indicating very small changes in the force field of the electronically excited singlet state relative to the ground state. The small changes of the a_{1g} vibrational frequencies between S_1 and S_0 are characteristic also of

TABLE V. The a_{1g} vibrational frequencies of linear polycenes (frequencies in cm^{-1}).

Naphthalene $N(a_{1g}) = 9$ Ref. (59)	Anthracene $N(a_{1g}) = 12$ Ref. (59)	Tetracene $N(a_{1g}) = 15$ (present work)	
S_0	S_0	S_0	S_1
		307	314
	369		
512			
	658		
		612	600
763	745	738	750
1025	1007	986	
1144	1169	1149	1159
	1240		1225
1379	1398	1381	1362
1460	1476	1442	1431
		1536	1529
1579	1584		1551
3025	3037		
3055	3053		
	3085		

lower linear polycenes, i.e., anthracene and naphthalene.[59] This normal behavior of the tetracene molecule drastically differs from the pattern exhibited by the isolated pentacene molecule,[40] which reveals a substantial change in the nuclear potential surface of the S_1 state.

From the comparison of the a_{1g} vibrational frequencies of the isolated tetracene molecule and of this molecule embedded in a variety of condensed phases (Tables II and V), we draw some conclusions regarding weak intermolecular medium perturbations of the a_{1g} vibrational frequencies of the tetracene molecule in the S_0 and in the S_1 electronic configurations. This general normal feature of the tetracene molecule drastically differs from the behavior of the larger linear polycene, i.e., the pentacene molecule, which exhibits a low-frequency nuclear motion in the S_1 state,[40] that is clamped by medium perturbations.

To obtain some further insight into the nature of the a_{1g} vibrational frequencies of the tetracene molecule, we have assembled in Table V the nine out of $N=15$ a_{1g} fundamentals of the tetracene molecule, which were identified on the basis of the present and previous work, together with the totally symmetric fundamentals for the S_0 state of naphthalene ($N=9$) and of anthracene ($N=12$). Some of the a_{1g} fundamental vibrations of the tetracene molecule are exhibited by the lower linear polycenes, thus providing additional support to the spectroscopic assignments of these fundamentals.

The results of the present detailed analysis of the vibrational structure of the isolated tetracene molecule are of interest because of three reasons. First, the close agreement between the vibrational structure of the isolated, ultracold, large molecule and the molecule in a condensed medium, which was rationalized in terms of the pedestrian argument concerning weak intermolecular perturbations, is of interest as it clearly demonstrates the reliability of the experimental methods developed by us for laser spectroscopy in supersonic beams. This credibility test will be of considerable importance to assess the reliability of new results concerning excited-state nuclear motion in larger isolated polycenes, which exhibit some isoteric effects. Second, our data provide additional information concerning relative intensities and, consequently, the Franck–Condon vibration overlap factors (Sec. IV F). This information cannot be obtained for low-temperature mixed crystal spectra, which are contaminated by broad phonon sidebands. Third, and most important, the identification of the vibrational structure in the S_1 state of the ultracold, isolated, large molecule provides the means for exploration of excited-state dynamics following photoselective excitation.

F. Franck–Condon factors

To obtain spectroscopic information concerning the S_1 potential surface, two conventional sources of information are required:

(1) Frequency changes. As we have discussed in Sec. IV D these changes are small.

(2) Distortions of the nuclear equilibrium configuration between the S_1 and the S_0 nuclear potential surfaces for the totally symmetric vibration. These distortions are readily obtained from the vibrational overlap factors in absorption and in emission. In view of the small frequency changes, the Franck–Condon nuclear vibrational overlap factors are essentially determined by the distortions of the equilibrium configuration upon electronic excitation. The Franck–Condon factors $f(0v_i'')$ for the transition $S_0(0)\rightarrow S_1(v_i'')$ are given by

$$f(0v_i'') = |\langle 0|v_i''\rangle|^2 , \tag{IV.1}$$

where $\langle 0|v_i''\rangle$ corresponds to the vibrational overlap integral. From the fluorescence excitation spectra (Figs. 6 and 7), we can evaluate the relative Franck–Condon factors from the simple relation

$$\frac{f(0v_i'')}{f(00)} = \left(\frac{A_{0\text{-}v_i''}}{A_{0\text{-}0}}\right)\left(\frac{\tau(0)}{\tau(v_i'')}\right) , \tag{IV.2}$$

where $A_{0\text{-}v_i''}$ and $A_{0\text{-}0}$ are the areas of the $0\rightarrow v_i''$ transition and of the $0\rightarrow 0$ transition in the fluorescence excitation spectrum, respectively; $\tau(0)$ and $\tau(v_i'')$ represent the experimental radiative decay lifetimes of the states $S_1(0)$ and $S_1(v_i'')$, respectively. The lifetime ratio in Eq. (IV.1) corresponds to the ratio of the fluorescence quantum yields from the vibronic components of an allowed electronic transition, as will be discussed in Sec. IV. Utilizing the relative intensities in the fluorescence action spectra, together with the experimental radiative lifetimes reported in Sec. VI, we have estimated the relative Franck–Condon factors $[f(01_i'')/f(00)]$ for the totally symmetric a_{1g} vibrations. For the 314 cm^{-1} vibration, we have taken the ratio of the areas of the corresponding spectral feature from Fig. 8, and for the higher-energy a_{1g} vibrations, we have taken the ratio of the amplitudes of the corresponding spectral feature and the 0–0 band as a rough measure of $A_{0\text{-}1_i''}/A_{0\text{-}0}$). An alternative way to estimate the Franck–Condon factors between the displaced potential surfaces S_1 and S_0 rests on the use of the relative intensities in the energy-resolved emission spectrum resulting from the $S_1(0)$ electronic origin. The Franck–Condon factors $f(0v_i')$ for the transitions $S_1(0)\rightarrow S_0(v_i')$ can be related to the Franck–Condon factors (IV.1) by the near quality

$$f(0v_i') \simeq f(0v_i'') , \tag{IV.3}$$

which is expected to be exact provided that the vibrational frequencies in the two electronic states are equal. In view of the small frequency changes between the S_1 and S_0 electronic states, the approximate relationship (IV.3) is expected to hold for the problem at hand. The Franck–Condon factors can thus be obtained also from the energy-resolved emission spectra from the relation

$$\frac{f(0v_i')}{f(00)} = \frac{B_{0\text{-}v_i'}}{B_{0\text{-}0}} , \tag{IV.4}$$

where $B_{0\text{-}v_i'}$ and $B_{0\text{-}0}$ correspond to the areas of the $0\rightarrow 0$ transition and of the $0\rightarrow v_i'$ transition in the energy-resolved emission spectrum, respectively. To obtain an accurate estimate of the intensity ratio (IV.4) for the 311 cm^{-1} ground state vibration, we display in Fig. 14 the two prominent lowest features in the energy-resolved emission from S_0 obtained under low resolution, and for other a_{1g} vibrations we have estimated the ratio (IV.4)

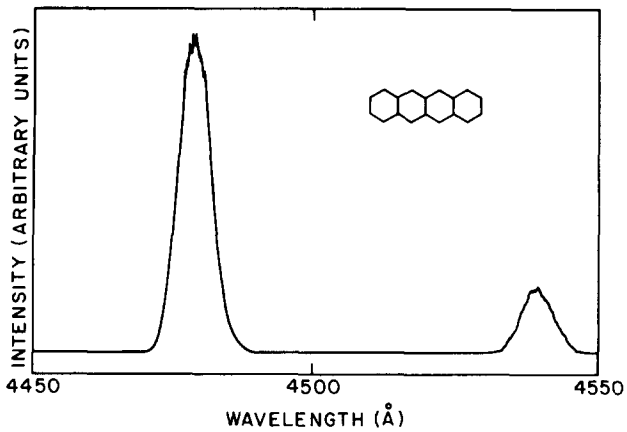

FIG. 14. Details of the energy-resolved fluorescence spectrum of Fig. 16 in the range 4450–4550 Å, which were used for the calculation of the relative vibrational overlap Franck–Condon factor for the ground state to the 311 cm^{-1} and the 314 cm^{-1} excited-state vibration.

from the amplitudes in the low resolution emission spectrum of Fig. 11. In Table VI, we present the results for the estimates of the Franck–Condon overlap factors $f(01_i'')/f(00)$ and $f(01_i')/f(00)$ for the prominent totally symmetric a_{1g} vibrations of tetracene. From the accurate data for the S_1 314 cm^{-1} vibration and for the S_0 311 cm^{-1} vibration, we get $f(01_i'')/f(00) = 0.21$ from the fluorescence action spectrum, together with lifetime data, and for the 311 cm^{-1} vibration in S_0 we obtain $f(01_i')/f(00) = 0.20$; the close agreement between the two sets of Franck–Condon factors demonstrates the validity of the propensity rule (IV.3). The agreement between the rough estimates of the relative Franck–Condon factors for other a_{1g} vibrations, obtained in Table VI from the two independent sets of experimental data, is as good as can be expected. In the last column of Table VI, we have displayed a mean value of the Franck–Condon factor for the a_{1g} vibrations. This Franck–Condon factor provides a direct measure of the displacement of the equilibrium nuclear configuration, d_i, for this particular normal mode normalized to the rms of the zero-point energy displacement $(\mu_i\,\omega_i/\hbar)^{1/2}$ in the normal mode. Here, μ_i denotes the reduced mass, and $\omega_i (\simeq \omega_i'' \simeq \omega_i')$ represents the frequency of the normal mode. The Franck–Condon factor for the fundamental a_{1g} vibrations can be expressed explicitly in terms of the first term of a Poissonian distribution

$$f(01_i) = \exp(-G_i)\,G_i \ ,$$

where

$$G_i = (d_i^2/2)/(\hbar/\mu_i\,\omega_i) \ .$$

Thus, the relative Franck–Condon factors (tabulated in Table VI) provide a direct determination of G_i. These reduced squared displacements provide a measure of the configurational change. The Debye–Weller factor for the entire configurational change between S_1 and S_0 is $G = \sum_i + G_i$ with the sum taken over all the a_{1g} modes. From Table VI it appears that G is of the order of unity, so that about 35% of the total intensity is in the 0–0 transition. We can conclude that the total configurational change between the S_1 and S_0 electronic configurations is relatively small. These reduced displacements are expected to provide important spectroscopic input data for estimates of the rates of nonradiative electronic relaxation between the S_1 and the S_0 states of this large molecule.

G. Spectral shifts

The observation of the electronic origin of the isolated tetracene molecule in a supersonic expansion makes it possible to provide quantitiative data concerning spectral shifts of the electronic origin of the $^1A_{1g} \rightarrow {}^1B_{2u}$ transition in mixed crystals. The position of the zero-phonon line, corresponding to the electronic origin of tetracene, is located at 20 274 cm^{-1} in p-terphynel,[53] at 20 246 cm^{-1} in anthracene,[51] and at 20 252 cm^{-1} in naphthalene,[52] as compared to the energy of 22 361 cm^{-1} of the electronic origin of the isolated molecule. The red spectral shifts of 2087 cm^{-1} for p-terphynel and 2110 cm^{-1} for both anthracene and naphthalene host crystals amount to approximately 10% of the total excitation energy. These red spectral shifts reflect the effects of dispersive interactions on the intense (oscillator strength $f \simeq 0.1$)[60,61] electronic transition.

V. INTRASTATE ANHARMONIC COUPLING

The understanding of intrastate coupling and intramolecular vibrational energy redistribution (IVR) within a single electronic configuration of an "isolated" large molecule is of considerable interest in the broad area of intramolecular dynamics.[5,15] The elucidation of the general problem of IVR within a level structure of a bound molecular manifold has to address the following central ingredients: (a) The specification of the level structure of the bound molecular eigenstates. (b) The characterization of the excitation amplitudes, i.e., the

TABLE VI. Nuclear vibrational overlap Franck–Condon factors between the S_1 and S_0 electronic states of tetracene.

Ground state frequency (cm^{-1})[a]	$\frac{f(01_i')}{f(00)}$[b]	Excited State frequency (cm^{-1})[c]	$\frac{f(01_i'')}{f(00)}$[d]	G_i[e]
307	0.20	314	0.21	0.21
612	0.01	600	0.02	0.015
738	0.05	750	0.05	0.05
986	0.03			0.03
1149	0.12	1159	0.10	0.11
		1225	0.10	0.10
1381	0.33	1362	0.15	0.24
1442	0.06	1431	0.13	0.09
1536	0.09	1529	0.05	0.07
		1551	0.12	(0.12)

[a] Accuracy ±10 cm^{-1}.
[b] Estimated from amplitude ratio in instrumentally broadened emission spectrum (resolution 20 cm^{-1}).
[c] Accuracy ±2 cm^{-1}.
[d] Franck–Condon factor (FCF) for 314±2 cm^{-1} vibration estimated from the relative areas of the 0–0 and the 314 cm^{-1} vibration in the fluorescence excitation spectra. All other FCF's are determined from the ratio of the amplitude of a given transition to the 0–0 excitation. The latter FCF's constitute a rough approximation, accurate within a numerical factor of two or so.
[e] G_i is the average of the FCF's for the ith a_{1g} mode obtained from the energy-resolved fluorescence and from the excitation spectra.

energy dependence of the distribution of oscillator strengths. (c) The definition of initial conditions which determine the dynamics of the molecular system. Spectroscopic data provide direct information concerning the level structure and the distribution of excitation amplitudes, while energy-resolved and time-resolved spectroscopy provide supplementary information concerning intramolecular dynamics. The current understanding of the intrastate level structure rests on the following description of the nuclear energy levels in the order of increasing energy[38,39]:

Range A. A sparse vibrational manifold where each vibratic level is well isolated from the others.

Range B. A vibrational quasicontinuum characterized by high density of states.

Theoretical intramolecular criteria for the location of the onset of the vibrational quasicontinuum in an isolated molecule rest on the conditions of (a) strong intrastate coupling $V_A\rho \gg 1$, where V_A is the anharmonic interaction between zero-order vibrational states and ρ is the density of these states, and (b) efficient sequential decay $\gamma\rho \gg 1$, where γ corresponds to the radiative decay width, i.e., fluorescent decay ($\gamma \sim 10^{-3}$–10^{-5} cm^{-1}) for the S_1 state and infrared decay ($\gamma \sim 10^{-8}$ cm^{-1}) for the S_0 configuration.

A. Spectra congestion in the S_1 state

The first spectroscopic criterion for the identification of the threshold in the lowest, spin-allowed, electronically excited state of a large molecule rests on the observation of a congested vibrational level structure in the fluorescence excitation spectrum. This criterion is of general applicability, being previously applied by us to the S_1 state of pentacene[36] and of ovalene.[37] The fluorescence excitation spectra of the "bare" tetracene molecule (Figs. 6 and 7) can be classified in the order of increasing excess vibrational energy E_V above the electronic origin as follows:

(1) *Range A*, spanning the energy region 4475–4260 A. This range exhibits well-separated vibronic bands, the vibrational level structure in the S_1 manifold being sparse. Range A spans the energy range $E_V \simeq 0$–1000 cm^{-1}. The upper limit for range A was determined on the basis of unique spectroscopic assignment of vibration levels.

(2) *Range B*. In the higher energy range below 4050 Å, or so, the spectrum of the ultracold tetracene molecule exhibits a congested level structure consisting of overlapping bands superimposed on a background. The congested level structure in the S_1 state of tetracene sets in at the excess vibrational energy of $E_V \gtrsim 1900$ cm^{-1}, which marks the onset of the vibrational quasicontinuum in the S_1 state of tetracene.

The observation of the onset of spectral congestion provides only a semiquantitative diagnostic criterion for the identification of the onset of the vibrational quasicontinuum because of two reasons. First, from the experimental point of view there is some ambiguity in the definition of the onset for the congested vibrational level structure, which is taken to correspond to the energy where the spacing between individual spectral features is lower than their (rotational) widths. As rotational widths are 2–3 cm^{-1} under our experimental circumstances the onset of spectral congestion corresponds roughly to an effective density of states of the order of approximately 1 cm for optically accessible levels. Second, from the point of view of general methodology, this spectroscopic technique is inadequate to probe the details of the "transition" from range A to range B, which is not abrupt but rather gradual. The upper limit for range A in the S_1 state was determined to be located at $E_V \approx 1000$ cm^{-1}, as only below this excess energy unique spectroscopic assignment of all the vibrational levels could be provided. The spectroscopic assignment of the vibrational level structure in the S_1 manifold, provided in Sec. IV D and summarized in Table I, points towards the identification of Fermi resonances in the energy range $E_V = 1000$–1900 cm^{-1}, typical examples being the three lines (9), (10), and (11) in the vicinity of 4250 Å (Fig. 11), as well as lines (16) and (17) in the vicinity of 4213 Å. In the energy range $E_V = 1000$–1900 cm^{-1}, between the upper limit of range A and the onset of the vibrational quasicontinuum, anharmonic mixing between zero-order (harmonic) states will prevail, being manifested in the appearance of Fermi resonances. This intermediate energy range, to which we shall refer to as AB, will still exhibit a reasonably sparse level structure in absorption spectroscopy. To overcome two difficulties inherent in our first spectroscopic criteria, i.e., the practical difficulty due to rotational broadening as well as the methodological difficulty due to the gradual fuzzy "transitions" from range A to range B, we have applied a second spectroscopic technique which rests on energy-resolved emission spectroscopy.

B. Energy-resolved emission spectroscopy

We have developed a new method for the identification of the onset for intrastate mixing within a vibrational manifold of an electronically excited state of a large, isolated, ultracold molecule, which rests on the following characteristics of the energy-resolved emission spectrum:

(1) *Range A*. Photoselective excitation of vibronic states is expected to result in a "normal" emission spectrum of a nearly harmonic large molecule, which exhibits small configurational changes between S_1 and S_0.

(2) *Range AB*. Photoselective excitation of states results in the splitting of the emission bands in the energy-resolved fluorescence spectrum. This splitting is a consequence of anharmonic coupling in a moderately sparse manifold,[39] where individual states can be photoselected. The threshold for the splitting in the energy-resolved emission spectrum marks the onset for effective anharmonic coupling.

(3) *Range B*. At higher excess vibrational energies, photoselective excitation results in broadening of the energy-resolved emission, marking the characteristics of the statistical limit[5,39] for intrastate mixing. This broadening effect was observed in the energy-resolved

emission for the S_1 state of phtalocyanine,[34] of ovalene,[37] and of naphthalene.[52] Figures 15–17 portray several energy-resolved emission spectra for excess vibrational energies in the range $E_V = 0-3250$ cm^{-1}. The energy-resolved emission spectrum, Fig. 15(a), resulting from excitation into the electronic origin is dominated by the $S_1(0) \rightarrow S_0(0)$ transition, as is appropriate for small configurational changes (see Sec. IV G) between the S_1 and the S_0 potential surfaces. The vibrational structure of the transitions $S_1(0) \rightarrow S_0(v')$ was analyzed in Sec. IV C. Excitation of the S_1 state at low excess vibrational energies, e.g., at $E_V = 314$ cm^{-1}, [Fig. 15(c)] results in emission spectra that are characterized by two central characteristics: (i) The position of the dominant spectral features coincides within ± 10 cm^{-1} with the $S_1(0) \rightarrow S_0(0)$ emission. (ii) There is no evidence for any intrinsic line broadening of the dominant feature, its line broadening being instrumental. The individual bands in the emission spectra Fig. 15(b) and 15(c) correspond to the transitions $S_1(v_i'') \rightarrow S_0(v_i' + \bar{v}')$, where the initial vibrational state is $v_i'' = 314 \pm 2$ cm^{-1} for Fig. 15(b) and $v_i'' = 750 \pm 2$ cm^{-1} for Fig. 15(c). The corresponding ground state frequencies are $v_i' = 310 \pm 10$ cm^{-1} for Fig. 15(b) and $v_i'' = 740 \pm 10$ cm^{-1} for Fig. 15(c). Thus, the prominent $\Delta v = 0$ features, corresponding to $v' = 0$ in Fig. 15(b) and (c), practically coincide with the 0–0 transition of Fig. 15(a). All the three emission spectra

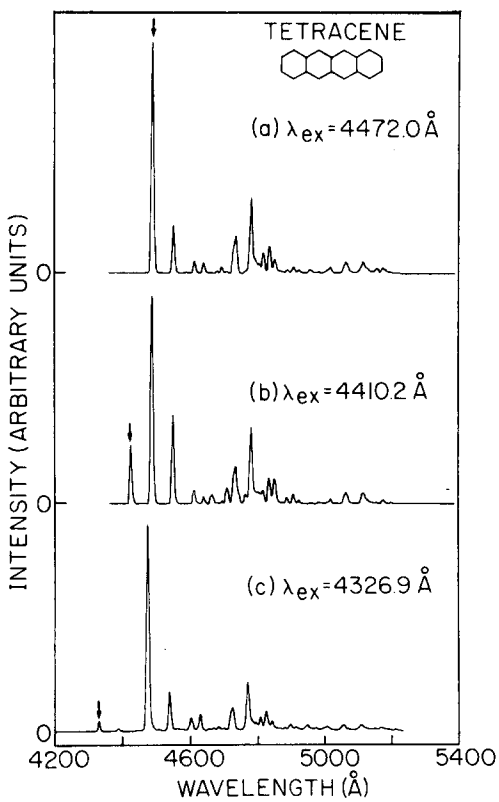

FIG. 15. Energy-resolved fluorescence spectra of tetracene cooled in a supersonic expansion (180 Torr Ar expanded through a 160-μ nozzle). Spectral resolution is 7 Å. Photoselective excitation was conducted at three laser wavelengths, corresponding to excess vibrational energies of (a) $E_V = 0$, (b) $E_V = 314$ cm^{-1}, and (c) $E_V = 750$ cm^{-1}. The laser wavelength is marked by an arrow. The resonance emission in all three spectra corresponds to genuine resonance fluorescence.

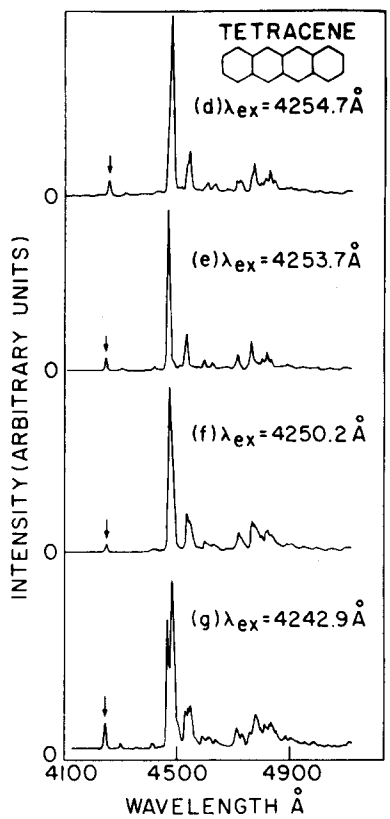

FIG. 16. Energy-resolved fluorescence spectra of tetracene under conditions as in Fig. 15. Photoselective excitation was conducted at four laser wavelengths at (d) $E_V = 1159$ cm^{-1}, (e) $E_V = 1168$ cm^{-1}, (f) $E_V = 1173$ cm^{-1}, and (g) $E_V = 1225$ cm^{-1}, which are portrayed in the lower part of Fig. 11. The resonance emission in the four spectra corresponds to genuine resonance fluorescence.

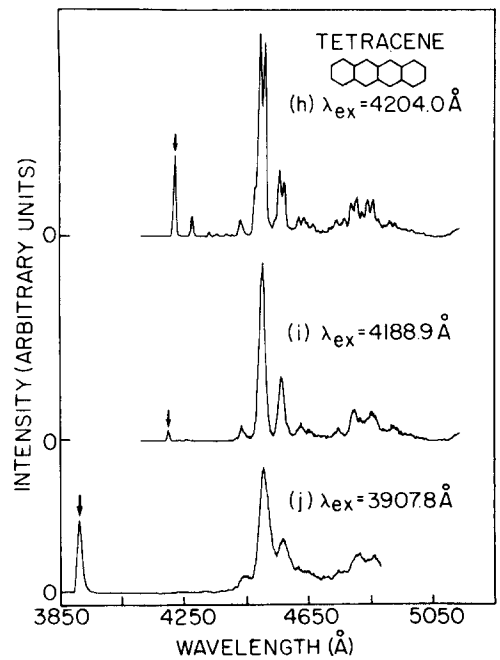

FIG. 17. Energy-resolved fluorescence spectra of tetracene under conditions as in Fig. 15. Photoselective excitation was performed at three wavelengths at (h) $E_V = 1442$ cm^{-1}, (i) $E_V = 1551$ cm^{-1}, and (j) $E_V = 3158$ cm^{-1}. The resonance emissions in (h) and (i) correspond to resonance fluorescence, and the resonance emission in (j) is spurious, being due to stray light.

of Fig. 15, resulting from photoselected S_1 states at $E_V \leq 750$ cm^{-1}, exhibit conventional spectroscopic features resulting from photoselection of a well-defined, nearly harmonic, initial vibrational state in the S_1 manifold. The energy range spanned in Fig. 15(a) clearly corresponds to the "A" region. Increase of the excess vibrational energy above 1000 cm^{-1} results in a dramatic change in the energy-resolved emission spectra, as is apparent from Figs. 16 and 17. Photoselection at $E_V = 1159$ cm^{-1} [Fig. 16(d)] and at $E_V = 1173$ cm^{-1} [Fig. 16(f)] results in the appearance of a shoulder on the $\Delta v = 0$ feature and other bands, and to an appreciable apparent broadening of the $\Delta v = 0$ feature. Excitation at $E_V = 1225$ cm^{-1} [Fig. 16(g)] and at $E_V = 1442$ cm^{-1} [Fig. 17(h)] results in a splitting of the $\Delta v = 0$ emission, as well as of other emission bands. This novel effect is attributed to the consequences of intermediate level structure within a single electronic manifold. Effective anharmonic mixing within a moderately sparse manifold results in scrambled nuclear molecular eigenstates, which are well separated in energy. As the level structure of these nuclear molecular eigenstates is sparse, a single nuclear molecular eigenstate (NME) can be photoselected, which can decay radiatively to a manifold of S_0 ground state NME's of the same vibronic parentage. Consequently, the $\Delta v = 0$ emission, as well as other vibrational transitions, will be split. The splitting of the emission bands provides a measure of the energetic spread of the scrambled NME's in the S_0 manifold. The appearance of splitting in the energy-resolved emission in the energy range 1000 cm$^{-1} \leq E_V \leq 1442$ cm^{-1} marks the AB transition range.

Additional increase of E_V above approximately 1500 cm^{-1} results in three effects on the $\Delta v = 0$ emission: (a) the disappearance of resolvable splitting, (b) appreciable broadening of the emission band, and (c) a large red shift of the peak of the $\Delta v = 0$ band relative to the 0–0 emission. Now, the density of scrambled NME's in the S_1 manifold is large. A wave packet of NME's is photoselected, each of which is radiatively coupled to a group of NME's of the S_0 manifold. This state of affairs corresponds to the statistical limit for intrastate coupling. This energy region corresponds to range B. Figures 18 and 19 provide an overview of the broadening, the splitting, and the spectral shift of the $\Delta v = 0$ feature in the energy-resolved emission from the S_1 manifold of the isolated tetracene molecule and provide detailed information regarding bound level structure of NME's for the tetracene molecule, which can be separated into three regions:

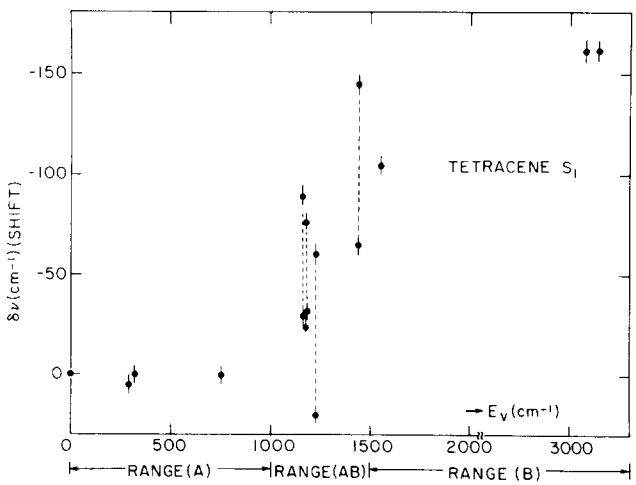

FIG. 18. The energy of the peak of the $\Delta v = 0$ band in the energy-resolved emission of tetracene in supersonic expansions of Ar is photoselectively excited at excess vibrational energies $E_V = 0$–3300 cm^{-1} above the electronic origin. The energies are displayed in terms of the spectral shift towards lower energies of the peak relative to the position of the 0–0 transition. When the $\Delta v = 0$ band is split, the positions of the two clearly resolved peaks were indicated and connected with a broken vertical line. The three distinct ranges A, AB, and B for intrastate scrambling are indicated.

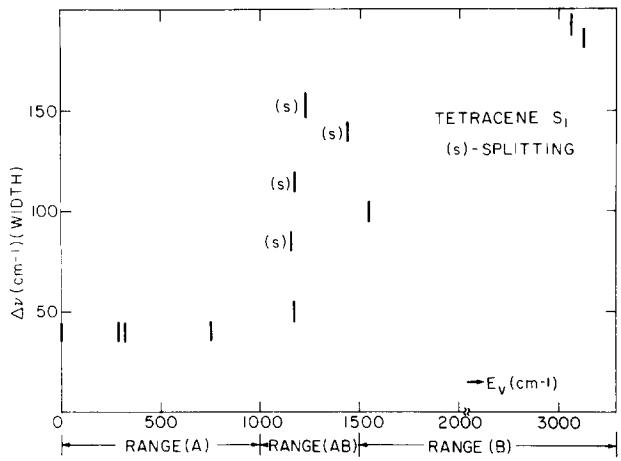

FIG. 19. The width (FWHM) of the peak of the $\Delta v = 0$ band in the energy-resolved emission of tetracene in supersonic expansions of Ar are photoselectively excited at excess vibrational energies $E_V = 0$–3300 cm^{-1} above the electronic origin. Splitting of the $\Delta v = 0$ band is indicated by (S). The three distinct ranges A, AB, and B for intrastate scrambling are indicated.

(I) Sparse level structure. Exhibited at a low excess vibrational energy $E_V < 1000$ cm^{-1}. Here both the absorption spectrum (Fig. 6) and the emission spectrum (Fig. 15) reveal well-separated spectral features, corresponding to uncontaminated vibrational levels.

(Ia) Intermediate level structure. In the energy range 1000 cm$^{-1} < E_V \leq 1500$ cm^{-1}, the absorption spectrum (Figs. 6 and 7) is still sparse, although on the basis of spectroscopic assignments (Sec. IV C) Fermi resonances can be identified. The emission spectrum (Figs. 16 and 17) manifests the effects of extensive anharmonic scrambling, resulting in a sparse distribution of NME's, all of which are individually active in absorption and in emission.

(II) The quasicontinuum. At excess vibrational energies $E_V > 1800$ cm^{-1}, the absorption spectrum exhibits a congested level structure, revealing overlapping bands superimposed on a background (Fig. 7). This congested level structure corresponds to overlapping resonances, which result from effective anharmonic mixing between a large number of close-lying zero-order vibrational states. This level structure can be considered as resulting from the effects of many-level Fermi resonances.

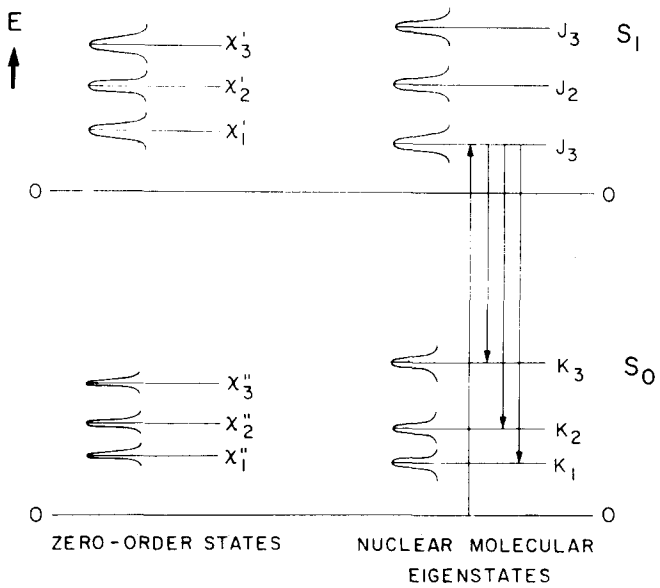

FIG. 20. A simple level structure for the splitting of emission in the intermediate energy region. The electronic origins of the S_0 and S_1 manifolds are labeled by zeros. Anharmonic interstate coupling V_A between the zero-order states in S_0 and between the zero-order states in S_1 results in the NME's labeled as $|K_i\rangle$ and $|J_j\rangle$ in the two electronic manifolds. In the intermediate level structure a single NMB, say $|J_3\rangle$, can be photoselected, which decays radiatively to all the $\{|K_i\rangle\}$ states of the same vibrational parentage.

In this energy range photoselection of an individual NME is practically impossible, and optical excitation results in a wave packet of S_1 NME's. When the absorption spectrum is reasonably uniform in energy, the dephasing of the initially excited wave packet will be fast on the time scale of the radiative decay, and individual uncorrelated NME's will be radiatively dumped.

C. Comments on energy-resolved fluorescence as a probe for intrastate dynamics

The dynamic implications of the spectroscopic results of the preceding section are of considerable interest as they bring up some central issues, e.g., level structure, transition amplitudes, and decay of scrambled NME's. To provide an adequate quantitative description of the energy-resolved emission, we shall utilize some results of the effective Hamiltonian formalism, which was developed to handle both time-resolved as well as energy-resolved observables.[3-5] The experiments described in Sec. V B correspond to energy-resolved observables, where the laser beam with frequency ω_1 is scattered from the molecular supersonic beam, and the scattered photons with energy ω_F are detected. To bring out the nature of the scrambled level structure, we should consider the NME's that are of the same vibrational parentage in S_1 and in S_0. These scrambled NME's, originating from anharmonic scrambling between zero-order nuclear states in the two electronic configurations, are portrayed in Fig. 20. Let us denote by $\{|\chi_\alpha'\rangle\}$ and by $\{|\chi_\beta''\rangle\}$ the zero-order vibrational states in the relevant energy region in the electronic configurations S_1 and S_0, respectively. Each χ_α' zero-order state is characterized by the energy E_α and decay width γ_α, and the χ_β'' states are characterized by energies E_β and decay width γ_β. We note in passing that the decay widths γ_α correspond to additive contributions from infrared decay, from radiative decay to the ground electronic state, as well as to electronic relaxation; the decay widths γ_β contain infrared decay only. Application of the effective Hamiltonian formalism[3,4,15-18] enables us to construct the NME's. These NME's $\{|J_j\rangle\}$ in the S_1 manifold are

$$|J_j\rangle = \sum_{\alpha=1}^{n} a_\alpha^j |\chi_\alpha'\rangle \ , \quad j = 1 \cdots n \ , \tag{V.1}$$

which are characterized by the energies $\epsilon(J_j)$ and decay width $\gamma(J_j)$. The mixing coefficients $\{a_\alpha^j\}$ are real for the intermediate level structure and complex in the statistical limit. Finally, n denotes the total number of the S_1 NME's in the relevant energy range. In a similar way, the NME's for the S_0 manifold are

$$|K_i\rangle = \sum_{\beta=1}^{n} b_\beta^i |\chi_\beta''\rangle \ , \quad i = 1 \cdots n \ , \tag{V.2}$$

being characterized by the energies $\epsilon(K_i)$ and widths $\gamma(K_i)$, the mixing coefficients being $\{b_\beta^i\}$. It is important to note that the mixing coefficients $\{a_\alpha^j\}$ and $\{b_\alpha^i\}$ in S_1 and in S_0, respectively, are usually different in the two electronic configurations. Finally, to complete the description of the level structure we have to incorporate the electronic origin $|g\rangle$ of S_0 characterized by the energy $E(g)$, which is the only populated ground state. The energy-resolved fluorescence is described in terms of a second-order process

$$|g\rangle \xleftarrow{H_{\rm int}} \{|J_j\rangle\} \xleftarrow{H_{\rm int}} \{|K_i\rangle\} \ , \tag{V.3}$$

involving radiative coupling, denoted by $H_{\rm int}$, between the S_0 origin $|g\rangle$ and the S_1 manifold $\{|J_j\rangle\}$, which is subsequently radiatively coupled to the S_0 manifold $\{|K_i\rangle\}$. The cross section $I_{K_i}(\omega_I, \omega_F)$ for the photon scattering process, where a photon ω_1 impinges on the molecule in state $|g\rangle$ resulting in a photon ω_F with the molecule in the state $|K_i\rangle$, is given by[3]

$$I_{K_i}(\omega_I, \omega_F) = \left| \sum_{J_j} \frac{\langle K_i | H_{\rm int} | \bar{J}_j \rangle \langle \bar{J}_j | H_{\rm int} | g \rangle}{E(g) + \hbar\omega_I - E(J_j) - i\gamma(J_j)/2} \right|^2 \times \delta(E(K_i) + \omega_F - E(g) - \hbar\omega_I) \ . \tag{V.4}$$

The total cross section $I(\omega_I, \omega_F)$ for the photon scattering process [Eq. (V.3)] is obtained by summing over all final NME's:

$$I(\omega_I, \omega_F) = \sum_{K_i} I_{K_i}(\omega_I, \omega_F) \ . \tag{V.5}$$

To obtain explicit expressions for the cross section, we shall invoke two reasonable assumptions. First, we assert that only a single zero-order state, say χ_1' in the S_1 manifold carries oscillator strength from $|g\rangle$, i.e., acts as a doorway state while all the other $\chi_\alpha'(\alpha \neq 1)$ states are inactive. The radiative coupling term connecting $|g\rangle$ and each $|J_j\rangle$, which appears in Eq. (V.4) can be expressed with the use of Eq. (V.1) in the following form:

$$\langle g | H_{\rm int} | J_j \rangle = a_1^j \langle g | H_{\rm int} | \chi_1' \rangle \ , \tag{V.6}$$

being determined by the amplitude of the doorway state. Second, as we are concerned with a molecule that exhibits relatively small configurational changes between S_1 and S_0, we can assume selective radiative coupling between zero-order states in the two electronic manifolds

$$\langle \chi'_\alpha | H_{\rm int} | \chi''_\beta \rangle = \mu \delta_{\alpha\beta} \ , \qquad (V.7)$$

where μ is some numerical constant. Consequently, the radiative coupling term connecting S_1 and S_0 NME's, which appears in Eq. (V.4), is given by

$$\langle K_i | H_{\rm int} | \bar{J}_j \rangle = \mu \sum_\alpha (a^j_\alpha)^* b^i_\alpha \ . \qquad (V.8)$$

Armed with Eqs. (V.4), (V.5), (V.6), and (V.8) the total scattering cross section takes the form

$$I(\omega_I, \omega_F) = |\mu|^2 |\langle \chi'_1 | H_{\rm int} | g \rangle|^2 \times \sum_{K_i} \left| \sum_{J_j} \frac{a^j_i \sum_\alpha (a^j_\alpha)^* b^i_\alpha}{E(g) + \hbar\omega_I - E(J_j) - i\gamma(J_j)/2} \right|^2 \times \delta[E(K_i) + \hbar\omega_F - E(g) - \hbar\omega_I] \ , \qquad (V.9)$$

which constitutes our general result. The cross section, Eq. (V.9), involves a generalized weighted density of states function, where the states at energies $[E(K_i) - E(g) + \hbar\omega_F - \hbar\omega_I]$ are weighted by a second-transition moment. This general result can readily be applied for the elucidation of the features of the intermediate level structure and the statistical limit.

(1) *Range AB.* Intermediate level structure. The level structure of the NME's is sparse, so that a single NME, say $|J_{\mathcal{K}}\rangle$, can be photoselected. The second-order transition moment in Eq. (V.9) contains a single term, so we get

$$I(\omega_I, \omega_F) \propto \sum_{K_i} \frac{|a^{\mathcal{K}}_i \sum_\alpha (a^{\mathcal{K}}_\alpha)^* b^i_\alpha|^2 [\gamma(J_{\mathcal{K}})/2]}{[E(J_{\mathcal{K}}) - E(g) - \hbar\omega_I]^2 + [\gamma(J_{\mathcal{K}})/2]} \times \delta[E(K_i) + \hbar\omega_F - E(g) - \hbar\omega_I] \ . \qquad (V.10)$$

From Eq. (V.10) it is apparent that the single NME $|J_{\mathcal{K}}\rangle$ decays radiatively to n final $\{|K_i\rangle\}$ levels in the S_0 manifold. The energy-resolved emission consists of n distinct components, resulting in the energetic splitting of the $\Delta v = 0$ emission. In particular, the following quantitative aspects of the energy-resolved emission spectrum equation (V.10), should be noted: (a) The energies of the components of the $\Delta v = 0$ emission for fixed $\hbar\omega_I$ and $\hbar\omega_F$ provides a direct measure of the energetic spread of the $\{|K_i\rangle\}$ NME's in the S_0 manifold. (b) The relative intensities of the components of the $\Delta v = 0$ emission are determined by the amplitudes $\{a^i_\alpha\}$ and $\{b^i_\beta\}$, which are governed by the intrastate anharmonic coupling.

(2) *Range B.* The statistical limit. The level structure of the NME's is now dense. Under these circumstances a single $|J_{\mathcal{K}}\rangle$ NME cannot be photoselected as the resonances overlap. The onset for overlap of resonances is exhibited when spacings become smaller than widths,

$$|E(J_j) - E(J_{j'})| \lesssim \gamma(E_j) \ , \ \gamma(E_{j'}) \ ,$$

for pairs of NME's. Now, the transition amplitudes in Eq. (V.9) contain a superposition from a large number of $\{|J_j\rangle\}$ NME's in the S_1 manifold and the contribution of interference terms. The broadened emission spectrum incorporates two major ingredients: (1) an energetic effect determined by the delta functions in Eq. (V.9), originating from the spread of the $\{|K_j\rangle\}$ NME's in the S_0 manifold and (2) the distribution of the transition amplitudes. The energetic broadening of the $\Delta v = 0$ emission resulting from photoselection in the statistical limit again reflects the energetic spread of the $\{|K_j\rangle\}$ ground state NME's. The red shift of the peak of the $\Delta v = 0$ emission apparently stems from different distributions of the mixing amplitudes $\{a^j_\alpha\}$ and $\{b^i_\beta\}$ in the two electronic configurations.

To conclude this discussion of the spectroscopic implications of intramolecular vibrational energy redistribution in the S_1 manifold of a large molecule, it is important to emphasize the universal features of intramolecular coupling and dynamics in a bound molecular level structure[5] manifested by the close analogy between the intrastate level structure considered herein and the well-established description of interstate coupling and electronic relaxation.[2-5,13,15]

VI. ELECTRONIC RELAXATION FROM THE S_1 MANIFOLD

We have studied the time-resolved fluorescence decay of tetracene seeded in supersonic expansion of Ar following photoselective excitation. The time-resolved emission of states at excess vibrational energies $E_V = 0$–4000 cm^{-1} was investigated. Typical experimental time-resolved decay curves are presented in Fig. 21. The time-resolved fluorescence exhibited a single exponential decay mode over two orders of magnitude. The decay lifetimes of the isolated ultracold molecule are summarized in Table I. The lifetimes τ of photoselected states at $E_V = 0$–4000 cm^{-1} drastically differ, both in respect to their absolute values and their E_V dependence, from the lifetimes of the S_1 state of tetracene obtained from low-pressure bulb experiments at room temperature.[63,64] The dramatic change in the lifetimes in the range of the electronic origin and the 314 cm^{-1} vibration upon cooling of the molecule is demonstrated in Fig. 22. The lifetimes of poorly defined initial states excited in the sequence bands of "hot" tetracene expanded in Ar at $p = 28$ Torr vary in the range $\tau = 5$–14 nsec. These relatively short lifetimes obtained herein by excitation of the "hot" molecule are in qualitative agreement with the lifetime data of Okajima and Lim[64] for this molecule in the bulb at 210 °C. This agreement between the present data for the hot molecule at $p = 28$ Torr and the bulb experiment[64] provides further credibility to the experimental techniques employed by us. Unfortunately, these decay lifetimes of the hot molecule[64] do not yield information concerning the lifetimes of well-defined photoselective vibrational states, as at high temperatures sequence congestion effects prohibit photoselective excitation, and the excited states correspond to considerably higher effective value of E_V.

The lifetimes summarized in Table I refer to the decay of states at photoselected well-defined values of E_V.

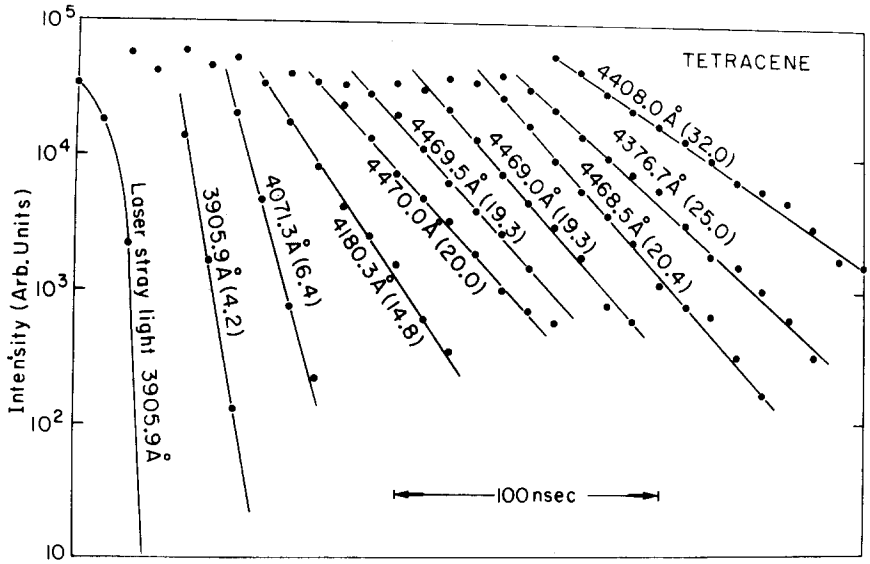

FIG. 21. Typical time-resolved radiative decay lifetimes of tetracene cooled in a supersonic expansion of 180 Torr Ar expanded through a 160-μ nozzle. The temporal Gaussian profile of the laser (marked laser stray light and measured in the absence of tetracene) is characterized by Eq. (II. 1). Note that the intensity of the laser stray light decreases by more than two orders of magnitude over a single Biomation (10 nsec) channel. The excitation wavelengths are marked on the lines. The lifetimes τ (in nsec) are also indicated on the lines.

In range A and range AB, well-defined vibrational states are photoselected and their subsequent decay is interrogated, whereas in range B the excitation involves a manifold of states in the vibrational quasicontinuum. We have failed to observe any dependence of the radiative decay lifetime on the rotational states. In an admittedly crude experiment the rotational envelope of the electronic origin was excited at four different energies, which correspond to energies of -3.0 cm^{-1}, -1.2 cm^{-1}, 0.8 cm^{-1}, and 2.8 cm^{-1}, relative to the center of the Q branch, i.e., the minimum of the double-humped rotational envelope. The decay lifetimes were in the range 19.3 ± 1 to 20.4 ± 1 nsec, being invariant (within the experimental uncertainty of 10%) to the nature of the photoselected group of rotational states.

In Fig. 22 we portray the dependence of the experimental fluorescent lifetimes τ of photoselected vibrational states within the S_1 manifold on the excess vibrational energy. These experimental decay lifetimes are determined by the well-known relationship

$$(\tau)^{-1} = (\tau_r)^{-1} + (\tau_{nr})^{-1} \ , \qquad \text{(VI. 1)}$$

where τ_r is the pure radiative lifetime, and τ_{nr} represents the nonradiative lifetime due to intramolecular electronic relaxation. In principle, both τ_r and τ_{nr} depend on the initially excited state. However, for a strongly allowed electronic transition, as is the case for the $S_0(^1A_{1g}) \rightarrow S_1(^1B_{2u})$ excitation of tetracene which exhibits only a small nuclear configurational distortion upon excitation, we expect that the pure radiative lifetime is only very weakly dependent on the initial vibrational state. For totally symmetric a_{1g} vibrational excitations (and their combinations) in the S_1 manifold, it is safe to assume that the electronic transition moment is constant and vibrational sum rules for all the radiative transitions $S_1(^1B_{2u}, a'_{1g}) \rightarrow S_0(^1A_{1g}, a''_{1g})$ taken over all the final vibrational states a''_{1g} do apply. According, the only dependence of τ_r on the initial vibrational state is due to the ν^3 factors (where ν is the frequency of photons emitted in each channel), which introduce a minor correction. For vibronically induced b_{3g} vibrational excitational excitations in the S_1 manifold, the major contribution to τ_r originates from the radiative transitions $S_1(^1B_{2u}; b'_{3g}) \rightarrow S_0(^1A_{1g}; b''_{3g} a''_{1g})$ with $b'_{3g} = b''_{3g}$, so that the approximate sum rule for all final a'_{1g} vibrational states does hold. We can thus conclude that the experimental τ data of Fig. 22 provide us with a measure of the gen-

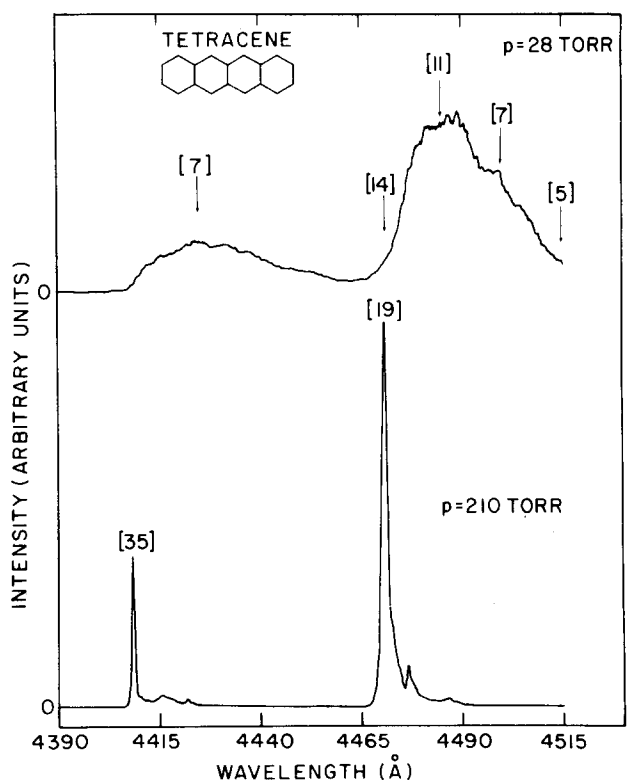

FIG. 22. The effect of sequence congestion of lifetimes of tetracene following photoselective excitation. The curves represent fluorescence excitation spectra of tetracene in Ar. The radiative decay lifetimes are denoted by numbers in square brackets [ ] and are given in nsec. Lifetimes were measured in the vicinity of the electronic origin and near the 314 cm^{-1} vibration. The upper curve with lifetimes in the range 5–14 nsec corresponds to "hot" tetracene expanded in Ar at $p = 28$ Torr. Under these circumstances, sequence congestion is severe. The lower curve corresponds to vibrationally cool tetracene expanded in Ar at $p = 210$ Torr.

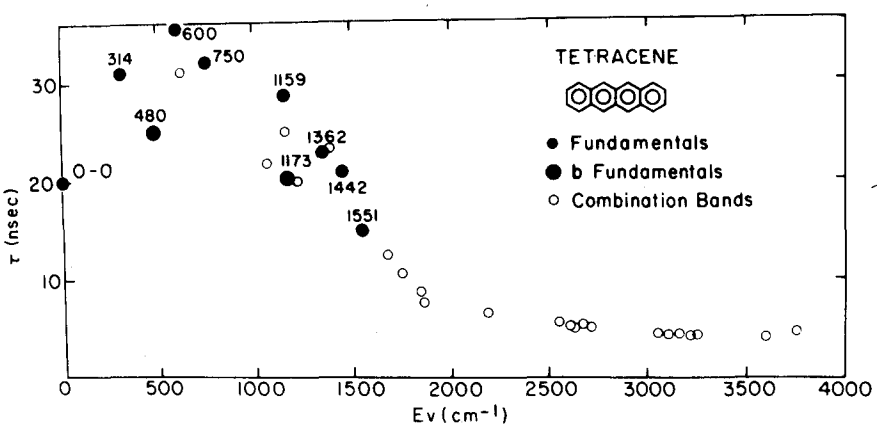

FIG. 23. Fluorescence decay lifetimes resulting from photoselective excitation of the isolated, ultracold, tetracene molecule cooled in a supersonic expansion ($p = 180$ Torr, $D = 150\ \mu$) of Ar. The lifetimes were found to be exponential, exhibiting a marked dependence for the excess vibrational energy E_V above the electronic origin, which was varied in the range $E_V = 0$–$4000\ \text{cm}^{-1}$.

eral trends of the nonradiative decay lifetimes for electronic relaxation. Our data provide quantitative information concerning the relative quantum yields for radiative decay. The quantum yield for fluorescent emissions is given by

$$Y = \tau/\tau_r \ . \qquad \text{(VI. 2)}$$

Provided that the pure radiative lifetime is practically independent of the initial state v_i'', the relative emission quantum yield $Y(v_i'')/Y(0)$ from the v_i state normalized to the emission yield from the electronic origin is just given by the ratio of the experimental decay lifetimes:

$$Y(v_i'')/Y(0) = \tau(v_i'')/\tau(0) \ . \qquad \text{(VI. 3)}$$

Strong experimental support for the validity of Eq. (VI. 3) and *vida infra* for the independence of τ_r on the initial state is obtained from the quantitative agreement between the Franck–Condon factors obtained in Sec. IV F (see Table VI) for the 314 cm^{-1} vibration from the fluorescence excitation spectra and from the energy-resolved emission. The relative emission quantum field from $v_i'' = 314\ \text{cm}^{-1}$ is obtained from the energy-resolved data of Sec. IV F in the form

$$Y(v_i'')/Y(0) = \left(\frac{A_{0\text{-}v_i''}}{A_{0\text{-}0}}\right)\left(\frac{B_{0\text{-}0}}{B_{0\text{-}v_i''}}\right) \ . \qquad \text{(VI. 4)}$$

Equation (VI. 4) yields the value $Y(v_i'')/Y(0) = 1.60 \pm 0.15$, which is in excellent agreement with the direct determination of the relative quantum yield, Eq. (IV. 3), which gives $Y(v_i'')/Y(0) = 1.59 \pm 0.15$ for the 314 cm^{-1} vibration.

The general features of the dependence of τ, and of the relative emission quantum yield, on the excess vibrational energy (Fig. 23) can be summarized as follows:

(1) The lifetimes and the relative emission yields increase with increasing E_V at low values of E_V, reaching a maximum at $E_V \sim 600\ \text{cm}^{-1}$. The experimental lifetimes of the 314 cm^{-1}, 600 cm^{-1}, and 750 cm^{-1} vibrational states are close to the pure radiative lifetime $\tau_R \sim 30$–35 nsec[65] estimated from the oscillator strength.[60,61]

(2) Excitation of vibrational fundamentals and their combinations at low excess vibrational energies $E_V = 0$–$1400\ \text{cm}^{-1}$ result in an increase of the experimental lifetime and in the enhancement of the emission quantum yield, as compared to their values at the electronic origin. Thus, at these low excess vibrational energies we observe retardation of the electronic relaxation rate, $(\tau_{nr})^{-1}$ with increasing E_V.

(3) In the energy range $E_V = 1500$–$2000\ \text{cm}^{-1}$, τ and the emission quantum yield decrease quite fast with increasing E_V, the relative emission quantum yield decreasing by a numerical factor of four in this energy range.

(4) In the high-energy range $E_V = 2000$–$4000\ \text{cm}^{-1}$, τ is practically constant, being independent of the excess vibrational energy.[66]

These experimental data provide central information concerning electronic relaxation from photoselected states in the S_1 manifold of the tetracene molecule. It is quite safe to assume that the only open decay channels in the energy range studied herein involve nonreactive electronic relaxation to lower electronic configurations, i.e., $S_1 \rightarrow T_1$ and $S_1 \rightarrow S_0$. It is reasonable to assume that both these channels correspond to the statistical limit for electronic relaxation. Unfortunately, direct information concerning the branching ratio between these channels is not yet available. Needless to say, such information has to be obtained for the isolated ultracold molecule. In what follows we shall have to invoke some untested and unsafe assumptions and conjectures to specify the decay channels. The two truly surprising features of our photoselective dynamic studies are the retardation of the electronic relaxation rate at low E_V and the practical independence of τ and of the electronic relaxation rate in E_V for high excess vibrational energies. Both observations are in contrast to most theoretical predictions.[15,17,18] We shall now proceed to discuss separately the features of the ER rate in the low and in the high E_V regions.

The retardation of the ER rate, relative to the ER dynamics of the electronic origin, is exhibited for $E_V = 0$–$1500\ \text{cm}^{-1}$. In particular, the surprising increase of τ with increasing E_V is exhibited for $E_V = 0$–$750\ \text{cm}^{-1}$. This energy region corresponds to range A, according to the classification of the level structure (Sec. V), where the S_1 vibrational level structure is sparse. In this energy range individual, nearly harmonic, vibronic levels are photoselected, and their interstate ER is sub-

sequently interrogated. In this low-energy range each vibronic level acts on its own and IVR is not exhibited, whereupon the molecule cannot act as its own heat bath. The dependence of the ER rate $\gamma_{nr}(E_V) = [\tau_r(E_V)]^{-1}$ on E_V in range A can be estimated on the basis of numerical model calculations based on the harmonic model for interstate decay of individual vibronic levels.[17] Three general trends for the dependence of $\gamma_{nr}(E_V)$ on E_V can be exhibited.[17] (a) For a large electronic energy gap relative to the characteristic vibrational frequencies, $\gamma_{nr}(E_V)$ exhibits a fast, nearly exponential increase with increasing E_V. (b) For moderate values of the electronic energy gap, $\gamma_{nr}(E_V)$ exhibits a moderate, close-to-linear increase with increasing E_V. (c) For small values of the electronic energy gap, $\tau_r(E_V)^{-1}$ initially decreases with increasing E_V, reaching a minimum and then starts increasing. This effect originates from the decrease of the nuclear Franck–Condon factors at small values of the energy gap with increasing E_V. The experimental observation of the retardation of the ER rate of photoselected states in the S_1 manifold of tetracene at low values of E_V can tentatively be accounted for in terms of $S_1 \rightarrow T_1$ intersystem crossing, which corresponds to case (c). This mechanism requires a small electronic energy gap between the electronic origins of the two electronic states. Two comments are in order at this point. First, from the point of view of methodology, the general mechanism proposed herein for $S_1 \rightarrow T_1$ intersystem crossing at low values of E_V is consistent with our recent observation of the heavy atom effect on ER of the electronic origin of low vibrational levels of tetracene–Kr_n and tetracene–Xe_n van der Waals complexes.[35] Second, from the practical point of view, the intersystem $S_1 \rightarrow T_1$ crossing may be intermediated by a T_2 electronic configuration lying closely to the electronic origin of S_1. The coupling of S_1 with T_2, which in turn is effectively coupled to a T_1 quasicontinuum, will provide the small energy gap required to account for the interesting retardation effect of the ER rate. However, no experimental or theoretical information is currently available to test this proposed mechanism.

The observation of the independence (or the very weak energy dependence) of τ on E_V in the high-energy range $E_V = 2000–4000$ cm^{-1} is interesting and intriguing. The experimental decay lifetimes in this energy range are 4.5 ± 0.5 nsec with a spread that is smaller than the experimental uncertainty. As in this range τ is considerably lower than the pure radiative lifetime, we can assert that the constant lifetime is practically equal to the nonradiative decay lifetime. Thus, our data imply that τ_{nr} is constant in this energy range. Two general comments concerning these data are in order. First, the independence of τ and of τ_{nr} on E_V for high values of E_V is exhibited also in the S_1 state of the pentacene molecule, where $\tau = 5.5 \pm 0.5$ nsec in the energy range $E_V = 1000–3000$ cm^{-1}.[67] Thus, the invariance of τ at high values of E_V is expected to be a general phenomenon in the S_1 state of very large molecules. Second, the onset for the independence of τ on E_V sets in at the threshold of the vibrational quasicontinuum. This observation establishes an interesting relation between interstate ER and intrastate scrambling. We can assert that in range B the ER decay rate is independent of the excess vibrational energy. The theoretical interpretation of the energy dependence of the nonradiative decay rate is fraught with difficulties as one has to consider the implications of effective intrastate anharmonic mixing on the interstate ER process. An extreme point of view will invoke the assumption that the "molecule acts as its own heat bath" so that a microcanonical thermal distribution is accomplished among all vibrational degrees of freedom.[68] Such an extreme approach will imply that the average energy, e, for each vibrational degree of freedom is $e = E_V/S$, where S is the total number of vibrational degrees of freedom. Thus, for tetracene at $E_V = 4000$ cm^{-1}, we get $e = 50$ cm^{-1}, so that the vibrational temperature is quite low. Such an extreme view of complete intramolecular vibrational distribution will imply that the nonradiative lifetimes in range B will be close to the nonradiative lifetime of the electronic origin. This conclusion does not concur with the experimental data as for the electronic origin $\tau_{nr} \sim 50$ nsec (estimated from the experimental value $\tau = 20$ nsec and taking $\tau_r = 35$ nsec), while in range B $\tau_{nr} \simeq 4.5$ nsec. Thus the molecule excited in range B does not act as a simple thermal bath. We conjecture that the weak dependence of τ and of the ER rate in range B originates from the effects of effective but selective intrastate anharmonic mixing involving a subset of the vibrational states. Such an interplay between nondemocratic selective intrastate scrambling and interstate ER in large molecules is of considerable experimental and theoretical interest, and, undoubtedly, many examples of such phenomena may be unveiled in the future.

[1] J. P. Byrne and I. G. Ross, Can. J. Chem. **43**, 3253 (1965).
[2] J. Jortner, S. A. Rice, and R. M. Hochstrasser, in *Advances in Photochemistry*, edited by B. O. Pitts and G. Hammond (Wiley, New York, 1969).
[3] S. Mukamel and J. Jortner, in *The World of Quantum Chemistry*, edited by R. Daudel and B. Pullman (Reidel, Boston, 1974), p. 145.
[4] S. Mukamel and J. Jortner, in *Molecular Energy Transfer*, edited by R. D. Levine and J. Jortner (Wiley, New York, 1975), p. 178.
[5] J. Jortner and R. D. Levine, in *Photoselective Chemistry, Advances in Chemical Physics*, edited by J. Jortner, R. D. Levine, and S. A. Rice (Academic, New York, 1981) (in press).
[6] D. S. McClure, in *Solid State Physics*, edited by F. Seitz and D. Turnbull (Academic, New York, 1959), Vol. 8, p. 1.
[7] E. V. Shpolskii, Sov. Phys. Usp. **5**, 522 (1962); **6**, 411 (1963).
[8] T. J. Aartsma and D. A. Wiersma, Phys. Rev. Lett. **36**, 1360 (1976).
[9] T. E. Orlowski and A. H. Zewail, J. Chem. Phys. **70**, 1390 (1979).
[10] K. K. Rebane, in *Impurity Spectra and Solids* (Plenum, New York, 1970).
[11] B. R. Henry and M. Kasha, Annu. Rev. Phys. Chem. **19**, 161 (1968).
[12] E. W. Schlag, S. Schneider, and S. F. Fischer, Annu. Rev. Phys. Chem. **22**, 465 (1971).
[13] K. F. Freed, Top. Curr. Chem. **31**, 105 (1972).
[14] B. R. Henry and W. Siebrand, Org. Mol. Photophys. **1**, 153 (1973).
[15] S. A. Rice, in *Excited States*, edited by E. C. Lim (Academic,

New York, 1975), Vol. II.
[16]J. Jortner and S. Mukamel, in *Excited States*, edited by E. C. Lim (Academic, New York, 1977), p. 58.
[17]J. Jortner and S. Mukamel, in *MTP Series in Science, Theoretical Chemistry*, edited by C. A. Coulson and A. D. Buckingham (Butterworth, London, 1976), Vol. 1.
[18]K. F. Freed, in *Radiationless Transitions in Molecules and Condensed Phases*, edited by F. K. Fong (Springer-Verlag, Berlin, 1976), p. 23.
[19]R. K. Sander, B. Soep, and R. N. Zare, J. Chem. Phys. **64**, 1242 (1976).
[20]R. Naaman, D. M. Lubman, and R. N. Zare, Chem. Phys. **32**, 17 (1978).
[21]A. Kantrowitz and T. Grey, Rev. Sci. Instrum. **22**, 328 (1951).
[22]K. P. Huber and A. E. Douglas, Quarterly Progress Report, National Research Council, Ottawa, Canada, Division of Pure Physics, Reports 161 (1963), (1964), and (1965).
[23]M. P. Sinha, A. Schultz, and R. N. Zare, J. Chem. Phys. **58**, 549 (1973).
[24]R. E. Smalley, B. L. Ramakrishna, D. H. Levy, and L. Wharton, J. Chem. Phys. **61**, 4363 (1974).
[25]R. E. Smalley, L. Wharton, and D. H. Levy, J. Chem. Phys. **63**, 4977 (1975).
[26]D. H. Levy, L. Wharton, and R. E. Smalley, in *Chemical and Biochemical Applications of Lasers* (Academic, New York, 1977), Vol. 2, p. 1.
[27]D. H. Levy, R. Wharton, and R. E. Smalley, Acc. Chem. Res. **10**, 139 (1977).
[28]P. S. H. Fitch, L. Wharton, and D. H. Levy, J. Chem. Phys. **69**, 3424 (1978).
[29]A. Amirav, U. Even, and J. Jortner, J. Chem. Phys. **71**, 2319 (1979).
[30]E. W. Schlag (private communication).
[31]S. M. Beck, M. G. Liverman, D. L. Monts, and R. E. Smalley, J. Chem. Phys. **70**, 232 (1979).
[32]S. M. Beck, D. L. Morris, M. G. Liverman, and R. E. Smalley, J. Chem. Phys. **70**, 1062 (1979).
[33]F. M. Behlen, N. MIkami, and S. A. Rice, Chem. Phys. Lett. Lett. **60**, 364 (1979).
[34]P. S. H. Fitch, L. Wharton, and D. H. Levy, J. Chem. Phys. **70**, 2019 (1979).
[35]A. Amirav, U. Even, and J. Jortner, Chem. Phys. Lett. **67**, 9 (1979).
[36]A. Amirav, U. Even, and J. Jortner, Opt. Comm. **32**, 266 (1980).
[37]A. Amirav, U. Even, and J. Jortner, Chem. Phys. Lett. **69**, 14 (1979) and J. Chem. Phys. **74**, 3145 (1981).
[38]A. Amirav, U. Even, and J. Jortner, Chem. Phys. **51**, 31 (1980).
[39]A. Amirav, U. Even, and J. Jortner, Chem. Phys. Lett. **71**, 12 (1980).
[40]A. Amirav, U. Even, and J. Jortner, Chem. Phys. Lett. **72**, 21 (1980).
[41]B. Soep and A. Tramer, Chem. Phys. Lett. **64**, 465 (1979).
[42]R. Campargue and B. Soep, Chem. Phys. Lett. **64**, 469 (1979).
[43]I. Oref and B. S. Rabinovitch, Accts. Chem. Res. **12**, 166 (1979).
[44]C. D. Cantrell, S. M. Freund, and J. L. Lyman, in *Laser Handbook* (North Holland, Amsterdam, 1979), Vol. III.
[45]N. Bloembergen and E. Yablonovitch, Phys. Today **31**, 23 (1978).
[46]R. Campargue and J. P. Breton, Entropie **42**, 18 (1971).
[47]N. Abauf, J. B. Fenn, and D. R. Miller, in Rarified Gas Dyn. Proc. Int. Symp. **5**, 1317 (1967).
[48]R. A. Larsen, S. K. Neoh, and D. R. Herschbach, Rev. Sci. Instrum. **45**, 1511 (1974).
[49]A. Ashkenas and F. S. Sherman, in *Rarefied Gas Dynamics*, edited by J. H. de Leeuw (Academic, New York, 1966), Vol. 2, p. 84.
[50]G. M. McClelland, K. L. Saenger, J. J. Valentini, and D. R. Herschbach, J. Phys. Chem. **83**, 947 (1979).
[51]J. W. Sidman, J. Chem. Phys. **25**, 122 (1956).
[52]A. V. Solov'ev, Izv. Akad. Nauk SSSR, Ser. Fiz. **24**, 737 (1960).
[53]N. Kruse and G. J. Small, J. Chem. Phys. **56**, 2985 (1972).
[54]R. Pariser, J. Chem. Phys. **24**, 250 (1954).
[55](a) G. Herzberg, in *Infrared and Raman Spectra of Polyatomic Molecules* (Van Nostrand, New York, 1945). (b) H. C. Allen Jr. and P. C. Cross, in *Molecular Vib. Rotors* (Wiley, New York, 1963).
[56]D. P. Craig, J. M. Hollas, N. F. Redies, and S. C. Wait, Proc. Cambridge Philos. Soc. **253**, 544 (1961).
[57]Y. Tomkiewicz, R. P. Groff, and P. Avakian, J. Chem. Phys. **54**, 4504 (1971).
[58]A. Amirav, U. Even, and J. Jortner, J. Chem. Phys. (in press).
[59]N. Neto, M. Scrocco, and S. Califano, Spectrochim. Acta **22**, 1981 (1966).
[60]A. Bree and L. E. Lyons, J. Chem. Soc. **1960**, S206.
[61]G. C. Morris, J. Mol. Spectrosc. **18**, 42 (1965).
[62]R. E. Smalley (private communication).
[63]G. R. Fleming, C. Lewis, and G. Porter, Chem. Phys. Lett. **31**, 33 (1975).
[64]S. Okajima and E. C. Lim, Chem. Phys. Lett. **37**, 403 (1976).
[65]I. B. Berlman, in *Handbook of Fluorescence Spectra* (Academic, New York, 1965).
[66]The experimental values of the decay lifetime in this energy range are $\tau = 4.5 \pm 0.5$ nsec. These short lifetimes are believed to be accurate within 15%. We believe that these quite short lifetimes recorded in the supersonic beam are accurate and reliable because of two reasons. First, numerical simulations using the characteristic Gaussian response of our interrogation system demonstrate that our procedure (see Sec. IIH is reliable for lifetimes exceeding 4 nsec. Second, the experimental lifetimes of the cold molecule at high values of E_V are in good agreement with the lifetimes of tetracene in the bulb.[64] As for high excess vibrational energies, the effects of sequence congestion are not crucial; the agreement between the present supersonic beam lifetimes and the bulb lifetimes[64] at high E_V provide a check for the validity of our lifetime data.
[67]A. Amirav, U. Even, and J. Jortner (to be published).
[68]S. H. Lim, J. Chem. Phys. **58**, 5760 (1973).